

# Performance Analysis of Fingerprint-Based Indoor Localization

Lyuxiao Yang, *Graduate Student Member, IEEE*, Nan Wu, *Member, IEEE*, Yifeng Xiong, *Member, IEEE*,  
Weijie Yuan, *Member, IEEE*, Bin Li, *Member, IEEE*, Yonghui Li, *Fellow, IEEE*,  
Arumugam Nallanathan, *Fellow, IEEE*

**Abstract**—Fingerprint-based indoor localization holds great potential for the Internet of Things. Despite numerous studies focusing on its algorithmic and practical aspects, a notable gap exists in theoretical performance analysis in this domain. This paper aims to bridge this gap by deriving several lower bounds and approximations of mean square error (MSE) for fingerprint-based localization. These analyses offer different complexity and accuracy trade-offs. We derive the equivalent Fisher information matrix and its decomposed form based on a wireless propagation model, thus obtaining the Cramér-Rao bound (CRB). By approximating the Fisher information provided by constraint knowledge, we develop a constraint-aware CRB. To more accurately characterize nonlinear transformation and constraint information, we introduce the Ziv-Zakai bound (ZZB) and modify it for adapt deterministic parameters. The Gauss-Legendre quadrature method and the trust-region reflective algorithm are employed to make the calculation of ZZB tractable. We introduce a tighter extrapolated ZZB by fitting the quadrature function outside the well-defined domain based on the Q-function. For the constrained maximum likelihood estimator, an approximate MSE expression, which can characterize map constraints, is also developed. The simulation and experimental results validate the effectiveness of the proposed bounds and approximate MSE.

**Index Terms**—Indoor localization, fingerprint-based localization, constraint-aware, Cramér-Rao bound, Ziv-Zakai bound.

## I. INTRODUCTION

GIVEN its ever-increasing social and commercial benefits, high-accuracy indoor localization is becoming critical for supporting ubiquitous location-based services (LBSs) in the Internet of Things (IoT) [1]–[6]. In advanced LBS scenarios, meter-level or even sub-meter-level accuracy is expected [6], [7].

Characterized by obstacles, signal fluctuation, noise, and environmental variations, indoor environments tend to be more complex than outdoor scenarios, making the global navigation satellite systems (GNSSs) unable to provide reliable

coverage [8]. To this end, various alternative technologies, such as light detection and ranging (LiDAR) [9], ultrawide bandwidth (UWB) [10], Bluetooth [11], ZigBee [12] and Wi-Fi [13] aided solutions, have been investigated. Due to the pervasive deployment of Wi-Fi infrastructures indoors, Wi-Fi-based localization has become an attractive solution [6]. Traditional trilateration localization approaches rely on line-of-sight (LoS) measurements, which are difficult to obtain with many obstacles and room partitions. To avoid the need for LoS measurements, the Wi-Fi fingerprint-based localization exploits the relationship between a position and its corresponding signal pattern, such as received signal strength (RSS) [13], which has become a promising method.

Existing works on RSS fingerprint-based localization have been focus on algorithm development, while its theoretical performance remains relatively scarce [14]–[20]. A question yet to be resolved remains: *What level of accuracy can fingerprint-based localization ultimately achieve?* As a parameter estimation problem, the accuracy of fingerprint-based localization can be measured by the mean squared error (MSE) and its lower bounds. Currently, there are two major challenges in theoretical MSE analysis: firstly, the lack of a comprehensive characterization of information flow from fingerprint database to users' positions; and secondly, the difficulty in characterizing the *a priori* or constraint knowledge and the nonlinear mapping between physical space and signal space.

The log-distance path loss (LDPL) model is a credible model for RSS measurements [21], [22]. The lower bounds of MSE for RSS range-based localization has been extensively studied based on the Cramér-Rao bound (CRB) [23], [24], which is the most widely used performance analysis metric in parameter estimation [25]. Since the CRB for RSS range-based localization can characterize the effect of the propagation parameters and the access point (AP) deployment, some studies suggest that it is also suitable for fingerprint-based localization [26], [27]. However, this analysis method cannot depict the relationship between the localization performance and the data fields in the fingerprint database, such as, the number of training data, the positions of reference points (RPs), the uncertainties of the recorded fingerprints, etc. To address this issue, based on the detection theory, the effects of the RP intervals and the sampling sizes at each RP on localization errors were discussed in [28] and [29], respectively. However, the analyzable factors of these studies are one-sided, and their depiction of localization errors is inaccurate because they

Lyuxiao Yang, Nan Wu, and Bin Li are with the School of Information and Electronics, Beijing Institute of Technology, Beijing 100081, China (e-mail: bitylx@bit.edu.cn; wunan@bit.edu.cn; binli@bit.edu.cn).

Yifeng Xiong is with the School of Information and Communication Engineering, Beijing University of Posts and Telecommunications, Beijing 100876, China (e-mail: yifengxiong@bupt.edu.cn).

Weijie Yuan is with the Department of Electrical and Electronic Engineering, Southern University of Science and Technology, Shenzhen 518055, China (e-mail: yuanwj@sustech.edu.cn).

Yonghui Li is with the School of Electrical and Information Engineering, The University of Sydney, Sydney, NSW 2006, Australia (e-mail: yonghui.li@sydney.edu.au).

Arumugam Nallanathan is with the School of Electronic Engineering and Computer Science, Queen Mary University of London, E1 4NS London, U.K. (e-mail: a.nallanathan@qmul.ac.uk).

only consider the nearest fingerprints. To establish a bound characterizing the effect of training data, the technique of [30] takes the grid size of RPs into account by employing a discrete model based on the nearest neighbor method. The method of [31] elucidates the role of training data in calibrating the path loss exponents for RSS-based localization. However, these approaches still cannot accurately depict the flow of position information from training data to user.

The fingerprint-based localization is a typical constraint-aware problem, in which the map information and the *a priori* knowledge of propagation parameters can be modeled as uniform distributions [32], [33]. The general CRB cannot be applied directly to this problem since the probability density function (PDF) of uniform distributions is not differentiable [34], [35]. Another issue is that the fingerprints are highly nonlinear with respect to the positions, hence the linearization operation in the CRB calculation results in severely inaccuracy when the signal-to-noise ratio (SNR) is low [36]. These motivate the application of other theoretic inequalities of MSE. Being substantially different from CRB, the Ziv-Zakai bound (ZZB) was derived from a detection theoretic reformulation of the MSE, relating the MSE to the probability of error of a binary hypothesis testing problem [37]. As a “global” bound based on integration of the probability of error, the ZZB is able to characterize *a priori* information, and is almost tight even under low SNR conditions. In [32], the ZZB has been introduced to model *a priori* map information for localization, and a semi-analytical expression was proposed. In [38], a new evaluation metric “reliability” was proposed according to a decision problem formulation of fingerprint-based localization, which can be seen as a quasi-ZZB. However, since the reliability is a metric independent of training data and constraints, the analysis based on the reliability is not comprehensive. In fact, due to the complexity of mapping, the application of ZZB for fingerprint-based localization remains an open and challenging issue.

The maximum likelihood (ML) estimator is asymptotically optimal for deterministic parameter estimation [25], while the fingerprint-based localization can be modeled as a constrained ML (CML) estimation problem. The asymptotic nature of ML estimators makes the MSE analysis of the CML estimator tractable, which provides another perspective. Several studies have analyzed the performance of the CML estimator with differentiable constraint functions [39], [40], which, however, are not suitable for constraint-aware localization. The method of [41] provides two perspectives for approximating the MSE of the CML estimator with non-differentiable constraints, which has the potential to be extended to fingerprint-based localization.

In this work, we present a series of novel advancements in the performance analysis of fingerprint-based localization. To characterize the relationship between localization performance and training data, we derive a Fisher information matrix (FIM) grounded in the LDPL model without presupposing known propagation parameters, and bring forth a closed-form expression of the equivalent FIM (EFIM) for the position. By using FIM to approximately characterize constraint information, we develop a constraint-aware CRB (CCRB).

To more accurately analyze all relevant factors, we propose a ZZB for addressing constraint knowledge and nonlinear mapping, and significantly mitigate its computational demands through the Gauss–Legendre quadrature [42] and the trust-region reflective (TRR) algorithm [43]. To tighten the ZZB further, we fit the complete quadrature function within all the integration interval by using Q-function, thus developing an extrapolated ZZB (EZZB). Based on a sub-optimal projection, we present an approximate MSE (AMSE) expression for the CML estimator, which can characterize map knowledge with lower complexity compared with ZZB. We demonstrate the superiority of the proposed bounds and AMSE through simulations and experiments, where they demonstrate marked improvements over existing benchmarks. For better clarity of illustration, the features of the proposed performance analysis method are boldly and explicitly contrasted to the existing contributions in Table I.

The main contributions of this paper are summarized as follows:

- We derive a closed-form expression of the EFIM for the position estimation based on the LDPL model, assuming all model parameters are unknown, which yields a CRB. With an approximation of FIM for constraint information, we develop a CCRB for fingerprint-based localization.
- We improve the ZZB for deterministic parameters to make it tighter and apply it to fingerprint-based localization. To reduce complexity, we employ the Gauss–Legendre quadrature and the TRR algorithm for approximating the ZZB.
- Starting from the MSE expression for estimation problems with Gaussian noise, we propose an extrapolation method by using Q-function to fit the quadrature function, thereby making the ZZB tighter. On this basis, we provide an EZZB for fingerprint-based localization.
- Using the asymptotic nature of ML estimators, we develop an AMSE expression for the CML estimator of fingerprint-based localization by using a suboptimal projection, which achieves a favorable tradeoff between accuracy and complexity.
- We develop a localization prototype based on commercial devices, and conduct extensive simulations and experiments for evaluating the proposed metrics. The results show that our methods are effective for quantitatively characterizing localization performance.

The remainder of this paper is organized as follows. Section III specifies the observation model and formulates the fingerprint-based localization problem. In Section IV, we derive the expression of the Fisher information and present two CRBs. In Section V, we develop a modified ZZB and its tighter extrapolation. In Section VI, an AMSE of the CML estimator is presented. The numerical and experimental results are shown in Section VII and Section VIII, respectively. Finally, our conclusions are drawn in Section IX.

*Notations:* The letters  $a$ ,  $\mathbf{a}$ ,  $\mathbf{A}$ , and  $\mathcal{A}$  represent scalars, vectors, matrices, and sets, respectively.  $\hat{a}$  denotes an estimate of the variable  $a$ .  $\tilde{a}$  indicates an item related to training data.  $\mathcal{N}(\mathbf{m}, \mathbf{V})$  denotes a Gaussian distribution with mean  $\mathbf{m}$  and

TABLE I  
CONTRASTING OUR WORK TO THE EXISTING CONTRIBUTIONS FOR PERFORMANCE ANALYSIS OF FINGERPRINT-BASED LOCALIZATION

	Performance Analysis Metrics	MSE Metric	Analyzable Factors				Solution Form
			AP	Training data	Map	Other constraints	
[26]	CRB	✓	✓	N/A	N/A	N/A	Analytical
[30]	Variant of CRB	✓	✓	Imprecise	N/A	N/A	Analytical
[31]	CRB	✓	✓	Partial	N/A	N/A	Analytical
[32]	Bayesian CRB	✓	N/A	N/A	✓	N/A	Analytical
	ZZB (stochastic), Weiss–Weinstein bound	✓	N/A	N/A	✓	N/A	Numerical
[28], [29]	Decision-dependent error	N/A	✓	Partial	N/A	N/A	Numerical
[38]	Reliability	N/A	✓	N/A	N/A	N/A	Numerical
Our work	CRB	✓	✓	✓	N/A	N/A	Analytical
	CCRB	✓	✓	✓	Approximate	Approximate	Analytical
	ZZB, EZZB (deterministic)	✓	✓	✓	✓	✓	Numerical
	AMSE of CML estimators	✓	✓	✓	Approximate	N/A	Semi-analytical

variance  $\mathbf{V}$ .  $\mathbf{0}_k$  and  $\mathbf{I}_k$  respectively represent a zero matrix and an identity matrix, both of size  $k$  by  $k$ . The operation  $a \rightarrow b$  means that  $a$  is substituted by  $b$ . The notation  $[\cdot]^T$  denotes the transpose of a matrix or vector;  $[\cdot]^{-1}$  denotes the inverse of a square matrix;  $|\cdot|$  denotes the absolute value of a scalar;  $\|\cdot\|$  denotes the Euclidean norm of a vector. The operator  $\text{tr}(\cdot)$  denotes the trace of a square matrix;  $\text{diag}(\cdot)$  denotes the diagonalization operator. The function  $p(\cdot)$  represents the PDF of a variable.  $\varepsilon(\cdot)$  represents the MSE of an estimator.  $\mathbf{J}(\cdot)$  and  $Z(\cdot)$  represent the FIM and the ZZB of a variable, respectively.  $\text{Pr}(\cdot)$  represents the probability of an event occurring.  $P_{\min}(\cdot)$  represents the probability of error of a binary hypothesis testing problem.  $\mathbb{E}(\cdot)$  denotes the expectation operator across all observations.  $\nabla_a(\cdot)$  denotes a symmetrical valley-filling operator centered around  $a$ .  $\mathbb{Q}(\cdot)$  represents the Q-function. The notations  $f(\cdot)$ ,  $g(\cdot)$ , and  $h(\cdot)$  are also employed to represent functions.

## II. RELATED WORK

### A. Fingerprint-Based Localization

Fingerprint-based localization techniques is pioneered by RADAR [13]. Existing RSS fingerprint-based localization methods can be broadly classified into deterministic, probabilistic, and deep learning-based ones. Traditional deterministic methods use the KNN approaches with signal similarity measurement criteria including Euclidean distance [13] and cosine similarity [44]. Additionally, some improved deterministic methods have employed algorithms such as support vector machine [45] and linear discriminant analysis [46]. Probabilistic methods, based on the Bayesian criterion, combine user-collected fingerprint and fingerprint database to find the most probable position. A typical method is Horus [47], and other algorithms utilize factor graphs [15] and Bayesian networks [48]. With the continuous advancement of intelligent algorithms, the localization methods based on deep learning have also been extensively researched [20], [49].

To reduce the effort involved in constructing the fingerprint database, the Gaussian process is a widely used semi-supervised method, which models the relationship between fingerprints and positions in a continuous space [16], [17]. Crowdsourcing is another feasible way to replace the costly site survey with involuntary user participation [50]. The methods of GraphIPS [51] and LiFS [18] employ multi-dimensional scaling algorithms to map distances to positions with graph formulation. Within the Bayesian framework, The methods of UCMA [19] and Zee [52] utilize hidden Markov models and particle filters, respectively, to estimate the positions of crowdsourcing data.

### B. Localization Performance Analysis

A CRB-based analysis framework for wideband localization is established in [23]. The analysis of performance limits and geometric properties of array localization based on the CRB is presented in [53]. The performance of cooperative localization is in-depth discussed in [54] for wideband systems and in [24] for massive networks, respectively. The fundamental tradeoff of integrated sensing and communications based on the CRB-rate region is discussed in [5]. For indoor localization, some bounds, which can depict the *a priori* knowledge provided by maps, are proposed in [32]. Disregarding applications as fingerprints, there have been many studies focused on the performance of RSS-based localization [31], [55]–[57].

For fingerprint-based localization, the CRB is leveraged to investigate how the number of APs and RSS gradients affect localization performance in [26] and [27]. The impact of the statistical characteristics of fingerprint database on localization performance is studied in [58]. Given a fingerprint database, an approximate probability distribution of localization error is developed using the concept of Voronoi diagrams in [59]. By viewing fingerprint-based localization as a decision problem, the reliability has been proposed to analyze the impact of the AP deployment on localization performance in [38]. On this basis, the effects of the RP intervals and the sampling sizes at each RP on localization errors are further discussed in [28] and [29], respectively.

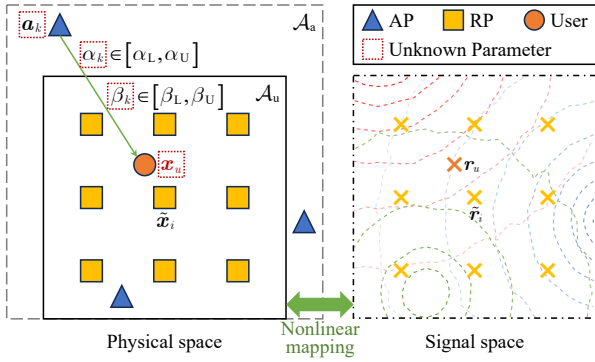


Fig. 1. Illustration of the fingerprint-based localization problem.

### III. SYSTEM MODEL

Fingerprint-based localization aims to estimate the positions of users based on the wireless fingerprint database (training data) and the user observations. The fingerprint database, denoted by  $\mathcal{D} = \{\{\tilde{\mathbf{r}}_i, \tilde{\mathbf{x}}_i\}, i = 1, 2, \dots, N_D\}$ , consists of multiple pairs of RSS vectors and the corresponding RP positions, while the user observation  $\mathbf{r}_u$  is the RSS vector obtained from the user's current position  $\mathbf{x}_u$ . Specifically, ignoring diacritical marks,  $\mathbf{r}_\cdot = [r_{\cdot,1}, r_{\cdot,2}, \dots, r_{\cdot, N_A}]^T$  are the RSS observations from  $N_A$  APs, and  $\mathbf{x}_\cdot = [x_\cdot, y_\cdot]^T$  is the 2-D physical coordinate. Assuming that all the RSS observations are collected in the same wireless propagation environment, according to the LDPL model, we have

$$r_{\cdot,k} = \alpha_k - 5\beta_k \lg \left[ (x_\cdot - a_k)^2 + (y_\cdot - b_k)^2 \right] + \omega_k, \quad (1)$$

where  $\mathbf{a}_k = [a_k, b_k]^T$  represents the position of the  $k$ -th AP,  $\alpha_k$  is the RSS at a distance of one meter away from the AP  $k$ ,  $\beta_k$  is the path loss exponent, and  $\omega_k \sim \mathcal{N}(0, \sigma_k^2)$  denotes a Gaussian random variable.

Let  $\mathcal{R} = \{\tilde{\mathbf{r}}_i\}$  and  $\mathcal{X} = \{\tilde{\mathbf{x}}_i\}$  respectively denote the sets of all RSS vectors and positions in  $\mathcal{D}$ . Define  $\boldsymbol{\kappa}$  as the vector of propagation parameters given by  $\boldsymbol{\kappa} = [\boldsymbol{\kappa}_1^T, \boldsymbol{\kappa}_2^T, \dots, \boldsymbol{\kappa}_{N_A}^T]^T$ , where  $\boldsymbol{\kappa}_k = [\alpha_k, \beta_k, a_k, b_k]^T$ . **Given these definitions and in the context of a constraint-aware scenario, a formulation of the fingerprint-based localization problem is as follows**

$$\arg \max_{\mathbf{x}_u} p(\mathbf{r}_u, \mathcal{R} | \mathbf{x}_u, \boldsymbol{\kappa}, \mathcal{X}) \quad (2a)$$

$$\text{s.t. } \mathbf{x}_u \in \mathcal{A}_u, \quad (2b)$$

$$\mathbf{a}_k \in \mathcal{A}_a, \quad (2c)$$

$$\alpha_L \leq \alpha_k \leq \alpha_U, \quad (2d)$$

$$\beta_L \leq \beta_k \leq \beta_U, \quad (2e)$$

In this formulation,  $\mathcal{A}_u$  and  $\mathcal{A}_a$  represent 2-D bounded regions associated with the users' accessible area and the AP deployment region, respectively. The values  $\alpha_L$  ( $\beta_L$ ) and  $\alpha_U$  ( $\beta_U$ ) denote the lower and upper bounds of  $\alpha_k$  ( $\beta_k$ ), respectively, which are informed by engineering experience. An illustration of the problem (2) is presented in Fig. 1.

The objective function in (2a) is the likelihood function with respect to  $\mathbf{x}_u$  and  $\boldsymbol{\kappa}$ , which can be further factorized as

$$p(\mathbf{r}_u, \mathcal{R} | \mathbf{x}_u, \boldsymbol{\kappa}, \mathcal{X}) = \prod_{k=1}^{N_A} \left[ p(r_{u,k} | \mathbf{x}_u, \boldsymbol{\kappa}_k) \prod_{i=1}^{N_D} p(\tilde{r}_{i,k} | \tilde{\mathbf{x}}_i, \boldsymbol{\kappa}_k) \right]. \quad (3)$$

From (1), both terms  $p(r_{u,k} | \mathbf{x}_u, \boldsymbol{\kappa}_k)$  and  $p(\tilde{r}_{i,k} | \tilde{\mathbf{x}}_i, \boldsymbol{\kappa}_k)$  are of the following form

$$p(r_{\cdot,k} | \mathbf{x}_\cdot, \boldsymbol{\kappa}_k) = \frac{1}{\sqrt{2\pi}\sigma_k} \times \exp \left\{ - \frac{\left\{ \alpha_k - 5\beta_k \lg \left[ (x_\cdot - a_k)^2 + (y_\cdot - b_k)^2 \right] - r_{\cdot,k} \right\}^2}{2\sigma_k^2} \right\}. \quad (4)$$

The optimal solution to (2) is a CML estimate [40]. When the constraints are not binding at the optimal solution, this estimator is asymptotically efficient [34], [36]. While obtaining exact CML solution remains intractable, we often turn to alternative approaches such as the  $K$  nearest neighbor (KNN) algorithms [13], Bayesian methods [15], Gaussian processes [16], and neural networks [60].

The primary performance metric for position estimation is the MSE, which is defined as

$$\varepsilon(\hat{\mathbf{x}}_u) = \mathbb{E} \left( \|\mathbf{x}_u - \hat{\mathbf{x}}_u\|^2 \right). \quad (5)$$

where  $\mathbb{E}(\cdot)$  denotes the expectation with respect to  $\mathbf{r}_u$  and  $\mathcal{R}$ . To establish benchmarks for localization algorithms and provide guidance for localization system deployment, it is crucial to derive the algorithm-independent performance limits, i.e., the lower bounds of MSE.

Our analysis of localization performance treats the position  $\mathbf{x}_u$  as a deterministic (non-random) parameter. This facilitates the evaluation of estimation performance across any position within  $\mathcal{A}_u$ , thereby enabling diverse optimization strategies. Such strategies could either aim to ensure ubiquitous localization accuracy across positions or focus on minimizing the average localization error. From the perspective of Bayesian inference for stochastic (random) parameters, the constraints (2b)–(2e) can be interpreted as *a priori* information characterized by uniform distributions [32]. Although the concept of “*a priori*” is broadly used in deterministic parameter estimation [36], [41], [61], to avoid confusion, we consistently use the term “constraint” for all parameters. Since there are unknown parameters  $\boldsymbol{\kappa}$  when estimating  $\mathbf{x}_u$ , we construct  $\boldsymbol{\theta}_u = [\mathbf{x}_u^T, \boldsymbol{\kappa}^T]^T$  as the complete parameter vector.

### IV. CRAMÉR-RAO BOUNDS

In the context of deterministic parameter estimation, the CRB serves as a prevalent analytical tool for assessing the asymptotic performance limits. According to [25], the FIM for  $\boldsymbol{\theta}_u$  is calculated by

$$\mathbf{J}(\boldsymbol{\theta}_u) = -\mathbb{E} \left[ \frac{\partial^2 \ln p(\mathbf{r}_u, \mathcal{R} | \boldsymbol{\theta}_u, \mathcal{X})}{\partial \boldsymbol{\theta}_u \partial \boldsymbol{\theta}_u^T} \right], \quad (6)$$

which can be written as a block matrix

$$\mathbf{J}(\boldsymbol{\theta}_u) = \begin{bmatrix} \mathbf{J}_{\mathbf{x}_u, \mathbf{x}_u} & \mathbf{J}_{\mathbf{x}_u, \boldsymbol{\kappa}} \\ \mathbf{J}_{\mathbf{x}_u, \boldsymbol{\kappa}}^T & \mathbf{J}_{\boldsymbol{\kappa}, \boldsymbol{\kappa}} \end{bmatrix}. \quad (7)$$

For the position  $\mathbf{x}_u$ , the MSE of any unbiased estimate  $\hat{\mathbf{x}}_u$  satisfies<sup>1</sup>

$$\varepsilon(\hat{\mathbf{x}}_u) \geq \text{tr}[\mathbf{J}_e^{-1}(\mathbf{x}_u)] \quad (8)$$

where  $\mathbf{J}_e(\mathbf{x}_u)$  is the EFIM for  $\mathbf{x}_u$  with respect to  $\boldsymbol{\theta}_u$ , which is calculated by

$$\mathbf{J}_e(\mathbf{x}_u) = \mathbf{J}_{\mathbf{x}_u, \mathbf{x}_u} - \mathbf{J}_{\mathbf{x}_u, \boldsymbol{\kappa}} \mathbf{J}_{\boldsymbol{\kappa}, \boldsymbol{\kappa}}^{-1} \mathbf{J}_{\boldsymbol{\kappa}, \mathbf{x}_u}^T. \quad (9)$$

According to (3), the FIM for the parameters  $\boldsymbol{\kappa}$  in (7) can be further partitioned as

$$\mathbf{J}_{\boldsymbol{\kappa}, \boldsymbol{\kappa}} = \begin{bmatrix} \mathbf{J}_{\boldsymbol{\kappa}_1, \boldsymbol{\kappa}_1} & \mathbf{J}_{\boldsymbol{\kappa}_1, \boldsymbol{\kappa}_2} & \cdots & \mathbf{J}_{\boldsymbol{\kappa}_1, \boldsymbol{\kappa}_{N_A}} \\ \mathbf{J}_{\boldsymbol{\kappa}_1, \boldsymbol{\kappa}_2}^T & \mathbf{J}_{\boldsymbol{\kappa}_2, \boldsymbol{\kappa}_2} & \cdots & \mathbf{J}_{\boldsymbol{\kappa}_2, \boldsymbol{\kappa}_{N_A}} \\ \vdots & \vdots & \ddots & \vdots \\ \mathbf{J}_{\boldsymbol{\kappa}_1, \boldsymbol{\kappa}_{N_A}}^T & \mathbf{J}_{\boldsymbol{\kappa}_2, \boldsymbol{\kappa}_{N_A}}^T & \cdots & \mathbf{J}_{\boldsymbol{\kappa}_{N_A}, \boldsymbol{\kappa}_{N_A}} \end{bmatrix}. \quad (10)$$

For the off-diagonal submatrices of  $\mathbf{J}_{\boldsymbol{\kappa}, \boldsymbol{\kappa}}$ , i.e., when  $k \neq l$ , we have

$$\mathbf{J}_{\boldsymbol{\kappa}_k, \boldsymbol{\kappa}_l} = -\mathbb{E} \left[ \frac{\partial^2 \ln p(\mathbf{r}_u, \mathcal{R} | \boldsymbol{\theta}_u, \mathcal{X})}{\partial \boldsymbol{\kappa}_k \partial \boldsymbol{\kappa}_l^T} \right] = \mathbf{0}_4, \quad (11)$$

where  $\mathbf{0}_4$  represents a  $4 \times 4$  matrix of all zeros. Therefore,  $\mathbf{J}_{\boldsymbol{\kappa}, \boldsymbol{\kappa}}$  is a block diagonal matrix. The matrix  $\mathbf{J}_{\mathbf{x}_u, \boldsymbol{\kappa}}$  denotes the contribution of the training data to the position information of user, given by

$$\mathbf{J}_{\mathbf{x}_u, \boldsymbol{\kappa}} = [\mathbf{J}_{\mathbf{x}_u, \boldsymbol{\kappa}_1} \quad \mathbf{J}_{\mathbf{x}_u, \boldsymbol{\kappa}_2} \quad \cdots \quad \mathbf{J}_{\mathbf{x}_u, \boldsymbol{\kappa}_{N_A}}]. \quad (12)$$

Due to the block-diagonal form of  $\mathbf{J}_{\boldsymbol{\kappa}, \boldsymbol{\kappa}}$ , we can simplify (9) into a form with lower computational complexity as

$$\mathbf{J}_e(\mathbf{x}_u) = \mathbf{J}_{\mathbf{x}_u, \mathbf{x}_u} - \sum_{k=1}^{N_A} \mathbf{J}_{\mathbf{x}_u, \boldsymbol{\kappa}_k} \mathbf{J}_{\boldsymbol{\kappa}_k, \boldsymbol{\kappa}_k}^{-1} \mathbf{J}_{\boldsymbol{\kappa}_k, \mathbf{x}_u}^T. \quad (13)$$

Based on (13), we derive the following result.

*Proposition 1 (EFIM for fingerprint-based localization):* When *Condition 1* is satisfied, the EFIM for  $\mathbf{x}_u$  is determined by

$$\mathbf{J}_e(\mathbf{x}_u) = \sum_{k=1}^{N_A} \gamma_{u,k} \mathbf{P}_{u,k}. \quad (14)$$

The matrix  $\mathbf{P}_{u,k}$  represents the nominal ranging information (NRI) provided by the  $k$ -th AP, which is calculated by

$$\mathbf{P}_{u,k} = \frac{\mathbf{u}_{u,k} \mathbf{u}_{u,k}^T}{\sigma_k^2}. \quad (15)$$

The scalar  $\gamma_{u,k}$  denotes the efficiency of training (EoT) in extracting the information of the  $k$ -th AP, which is calculated by

$$\gamma_{u,k} = \frac{1}{1 + \mathbf{s}_{u,k}^T \left( \tilde{\mathbf{S}}_k \tilde{\mathbf{S}}_k^T \right)^{-1} \mathbf{s}_{u,k}}. \quad (16)$$

<sup>1</sup>This formula applies only when the user is localizable (typically requiring  $N_A \geq 3$ ), and all the propagation model parameters can be determined by the training data.

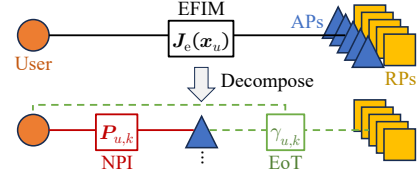


Fig. 2. Illustration of the decomposition of the EFIM for fingerprint-based localization.

The entities  $\mathbf{u}_{u,k}$ ,  $\mathbf{s}_{u,k}$  and  $\tilde{\mathbf{S}}_k$  are given by (44), (57) and (58), respectively.

*Proof:* Please refer to Appendix A.

*Condition 1:* There exist at least 4 distinct RPs such that any AP and these RPs are not all collinear, while for the 4 distinct RPs, one of the following conditions holds:

- There are at least 2 sets of RPs with different distances to any AP, and these 4 RPs are not all collinear.
- There are at least 4 sets of RPs with different distances to any AP.

According to (44), (57) and (58), the decomposition of the EFIM is presented in Fig. 2, with the lines connected to the NRI and EoT indicating the factors that influence their values. The NRI  $\mathbf{P}_{u,k}$  is a fundamental factor determining fingerprint-based localization performance, which is related to the user's position, the AP's position and its corresponding path loss exponent. The NRI indicates the strength and direction of the ranging information that each AP can provide to the user. To obtain 2-D position information, the superposition of the NRI from at least two APs is necessary, which has been investigated in [53]. The EoT  $\gamma_{u,k}$  is a novel concept introduced in fingerprint-based localization, determined by the relative position relationships among the user, the AP and all the training data. It is a scalar ranging from 0 to 1. When the number of training data approaches infinity, the value of  $\gamma_{u,k}$  asymptotically converges to 1. In fact, when  $\gamma_{u,k} = 1$ , (14) will degenerate into the EFIM of RSS range-based localization. Compared to the lack of characterization of training data in [26] and the inaccurate portrayal in [30] and [31], the proposed CRB comprehensively and accurately characterizes the impact of training data on localization performance using the EoT concept.

For optimizing the deployment of localization systems, considering the complexity and the fact that the deployment of APs and RPs usually occurs in different stages, it is necessary to provide separate optimization strategies for them. Conveniently, the NRI and the EoT respectively provide the basis for the optimization of AP and RP deployment. Particularly in scenarios where the APs have already been deployed, optimizing the spatial arrangement of RPs based on EoT might be an effective low-complexity approach.

The CRB derived above is not tight enough under low SNR conditions. Existing research indicates that the ambiguity phenomenon in localization is not significant when the localizability conditions are satisfied [62]. This suggests that the main factor affecting the accuracy of the CRB may not be its "localness" but rather its disregard for nonlinearity and constraints. Hence, there is an opportunity to improve the

CRB by utilizing the constraint information. Drawing from the approach of [32], we can present the FIM for  $\theta_u$  of the CCRB based on the approximate Fisher information of constraints as follows

$$\mathbf{J}_c(\theta_u) = \mathbf{J}(\theta_u) + \mathbf{J}_a(\theta_u), \quad (17)$$

where  $\mathbf{J}(\theta_u)$  is as shown in (7), and  $\mathbf{J}_a(\theta_u)$  is a diagonal matrix depicting the constraint knowledge. The matrix  $\mathbf{J}_a(\theta_u)$  has the following block diagonal form

$$\mathbf{J}_a(\theta_u) = \begin{bmatrix} \mathbf{J}_a(\mathbf{x}_u) & & & \mathbf{0} \\ & \mathbf{J}_a(\boldsymbol{\kappa}_1) & & \\ & & \ddots & \\ \mathbf{0} & & & \mathbf{J}_a(\boldsymbol{\kappa}_{N_A}) \end{bmatrix}. \quad (18)$$

Similar to (13), we can derive the EFIM for  $\mathbf{x}_u$  incorporating constraint information as follows

$$\mathbf{J}_c(\mathbf{x}_u) = [\mathbf{J}_{\mathbf{x}_u, \mathbf{x}_u} + \mathbf{J}_a(\mathbf{x}_u)] - \sum_{k=1}^{N_A} \mathbf{J}_{\mathbf{x}_u, \boldsymbol{\kappa}_k} [\mathbf{J}_{\boldsymbol{\kappa}_k, \boldsymbol{\kappa}_k} + \mathbf{J}_a(\boldsymbol{\kappa}_k)]^{-1} \mathbf{J}_{\mathbf{x}_u, \boldsymbol{\kappa}_k}^T. \quad (19)$$

When  $\mathcal{A}_u$  is a rectangle with the x-coordinate ranging between  $[x_L, x_U]$  and the y-coordinate ranging between  $[y_L, y_U]$ ,  $\mathbf{J}_a(\mathbf{x}_u)$  is calculated by

$$\mathbf{J}_a(\mathbf{x}_u) = \text{diag} \left[ \frac{c_m}{(x_U - x_L)^2}, \frac{c_m}{(y_U - y_L)^2} \right]. \quad (20)$$

Meanwhile, when  $\mathcal{A}_a$  is a rectangle with the x-coordinate ranging between  $[a_L, a_U]$  and the y-coordinate ranging between  $[b_L, b_U]$ ,  $\mathbf{J}_a(\boldsymbol{\kappa}_k)$  is calculated by

$$\mathbf{J}_a(\boldsymbol{\kappa}_k) = \text{diag} \left[ \frac{c_m}{(\alpha_U - \alpha_L)^2}, \frac{c_m}{(\beta_U - \beta_L)^2}, \frac{c_m}{(a_U - a_L)^2}, \frac{c_m}{(b_U - b_L)^2} \right]. \quad (21)$$

In (20) and (21), the constant  $c_m$  is equal to 4 for deterministic parameter estimation [41]. If we only consider the map constraint for  $\mathbf{x}_u$ , the CCRB will degenerate to the map-aware CRB (MCRB), leading to a more concise expression of the EFIM

$$\mathbf{J}_m(\mathbf{x}_u) = \mathbf{J}_e(\mathbf{x}_u) + \mathbf{J}_a(\mathbf{x}_u), \quad (22)$$

where  $\mathbf{J}_e(\mathbf{x}_u)$  is as shown in (14).

## V. ZIV-ZAKAI BOUNDS

In this section, we first present a definition of the ZZB suitable for deterministic parameters and extend it to fingerprint-based localization. Then, we propose a tighter EZZB based on the Q-function fitting.

### A. ZZB for Deterministic Parameters

Compared to the asymptotically achievable CRB, the ZZB is tighter under low SNR conditions. However, it's noted that the classical ZZB is defined for stochastic (random) parameters. Since we want to obtain a lower bound for the specific value  $\mathbf{x}_u$ , it is necessary to modify the definition of ZZB to accommodate deterministic parameters.

*Proposition 2 (ZZB for deterministic scalar parameters):* Consider an unknown parameter  $\theta$  with lower and upper bounds given by  $\theta_L$  and  $\theta_U$ , respectively. The  $i$ -th observation is

$$x_i = f(\theta, \mathbf{t}_i) + \omega_i, \quad (23)$$

where  $f(\theta, \mathbf{t}_i)$  is a function of  $\theta$ ,  $\mathbf{t}_i$  denotes other known parameters, and  $\omega_i$  is the observation noise. The MSE of any estimator for  $\theta$  satisfies

$$\varepsilon(\hat{\theta}) \geq \frac{1}{2} \int_{\theta_L}^{\theta_U} \nabla_{\theta} [P_{\min}(\theta, \varphi)] |\varphi - \theta| d\varphi, \quad (24)$$

where  $P_{\min}(\theta, \varphi)$  denotes the minimum probability of error for the following binary hypothesis testing problem

$$\begin{aligned} \mathbf{H}_0 : x_i &= f(\theta, \mathbf{t}_i) + \omega_i, & i = 1, 2, \dots, N \\ \mathbf{H}_1 : x_i &= f(\varphi, \mathbf{t}_i) + \omega_i, & i = 1, 2, \dots, N \end{aligned} \quad (25)$$

with  $\Pr(\mathbf{H}_0) = \Pr(\mathbf{H}_1) = 0.5$ .

*Proof:* Please refer to Appendix B.

Subsequently, drawing inspiration from the method of [37], we extend the ZZB for scalar parameters to the vector cases.

*Proposition 3 (ZZB for deterministic vector parameters):* Consider an unknown parameter  $\boldsymbol{\theta} = [\theta_1, \theta_2, \dots, \theta_K]^T$ . The lower and upper bounds of  $\theta_k$  are  $\theta_{L,k}$  and  $\theta_{U,k}$ , respectively. The  $i$ -th observation is

$$x_i = f(\boldsymbol{\theta}, \mathbf{t}_i) + \omega_i, \quad (26)$$

where  $f(\boldsymbol{\theta}, \mathbf{t}_i)$  is a function of  $\boldsymbol{\theta}$ ,  $\mathbf{t}_i$  denotes other known parameters, and  $\omega_i$  is the observation noise. The MSE of any estimator for  $\theta_k$  satisfies

$$\varepsilon(\hat{\theta}_k) \geq \frac{1}{2} \int_{\theta_{L,k}}^{\theta_{U,k}} \nabla_{\theta_k} \left[ \max_{\boldsymbol{\varphi}: \mathbf{w}_k^T \boldsymbol{\varphi} = \varphi} P_{\min}(\boldsymbol{\theta}, \boldsymbol{\varphi}) \right] |\varphi - \theta_k| d\varphi \quad (27)$$

where  $\mathbf{w}_k$  is a  $K$ -dimensional column vector with one at the  $k$ -th position and zeros elsewhere,  $P_{\min}(\boldsymbol{\theta}, \boldsymbol{\varphi})$  denotes the minimum probability of error for the following binary hypothesis testing problem

$$\begin{aligned} \mathbf{H}_0 : x_i &= f(\boldsymbol{\theta}, \mathbf{t}_i) + \omega_i, & i = 1, 2, \dots, N \\ \mathbf{H}_1 : x_i &= f(\boldsymbol{\varphi}, \mathbf{t}_i) + \omega_i, & i = 1, 2, \dots, N \end{aligned} \quad (28)$$

with  $\Pr(\mathbf{H}_0) = \Pr(\mathbf{H}_1) = 0.5$ .

*Proof:* Please refer to Section II-B in [37].

Our modified ZZB offers a more straightforward implementation for deterministic parameter estimation problems with defined lower and upper bounds, compared to the formula without specified integration limits in [63] and the complex-structured expression with a loose integration limit in [36]. The proposed ZZB is tighter as it accounts for the possibility of misjudgment at both ends of the true value.

The MSE for fingerprint-based localization, represented by the complete parameter vector, is given as

$$\varepsilon(\hat{\mathbf{x}}_u) = \mathbb{E} \left( \left| \mathbf{w}_x^T \hat{\boldsymbol{\theta}}_u \right|^2 \right) + \mathbb{E} \left( \left| \mathbf{w}_y^T \hat{\boldsymbol{\theta}}_u \right|^2 \right), \quad (29)$$

where  $\mathbf{w}_x = [1, 0, 0, \dots, 0]^T$   $\mathbf{w}_y = [0, 1, 0, \dots, 0]^T$  are the unit vectors corresponding to  $x$  and  $y$ , respectively. Based on Proposition 3, we can derive the lower bounds for both terms in (29), leading us to obtain the following result.

*Proposition 4 (ZZB for fingerprint-based localization):* For the position  $\mathbf{x}_u$ , the MSE of any estimate  $\hat{\mathbf{x}}_u$  satisfies

$$\varepsilon(\hat{\mathbf{x}}_u) \geq Z_x(\mathbf{x}_u) + Z_y(\mathbf{x}_u), \quad (30)$$

where  $Z_x(\mathbf{x}_u)$  and  $Z_y(\mathbf{x}_u)$  are calculated as (31), with subscript  $z$  representing  $x$  or  $y$  uniformly. In (31), the function  $f(\mathbf{x}_i, \boldsymbol{\kappa}_k)$  is defined as (75),  $z_L$  and  $z_U$  respectively represent the possible lower and upper bounds, and the unit vector  $\mathbf{w}_z$  denotes  $\mathbf{w}_x$  or  $\mathbf{w}_y$ .

*Proof:* Please refer to Appendix C.

There exists a nonlinear optimization problem inside the integral in (31), whose constraints include not only  $\mathbf{w}_z^T \boldsymbol{\theta}'_u = z$  but also (2b)–(2e) with the substitution  $\boldsymbol{\theta}_u \rightarrow \boldsymbol{\theta}'_u$ . To mitigate the computational overhead of repeatedly solving this optimization, we employ the Gauss–Legendre quadrature method to provide a numerical solution. This method employs the roots of Legendre polynomials to approximate integrals via weighted sums, allowing for high integration precision with few sample points. For the embedded optimization problem, we use the TRR algorithm, which is particularly adept at addressing problems constrained solely by boundary constraints. By striking a balance between the trust region and reflective steps, it can provide efficient and accurate solutions. However, due to the high-dimensional and nonlinear nature of the problem, the gradient-based TRR algorithm may converge to a local optimum, potentially leading to a bound that is not sufficiently tight. To address this, we introduce the true value of  $\boldsymbol{\theta}_u$  as the initial value for  $\boldsymbol{\theta}'_u$  in its optimization process. This strategy is intended to minimize the objective function of the optimization problem specified in (31).

As a global bound, the ZZB is applicable in scenarios that do not satisfy localizability condition and Condition 1. From (31), it is evident that the performance of fingerprint-based localization is actually related to  $\alpha_k$ , which can be considered as the transmission power. This differs from what the Fisher information, presented in (14), suggests. This discrepancy arises because the Fisher information only accounts for the local sharpness of the likelihood function, which is independent of  $\alpha_k$ . In fact, since the transmission power and path loss can be freely combined to produce the same observation (i.e. ambiguity phenomenon [36]), all free unknown parameters, including  $\alpha_k$ , have implications for the localization performance.

$$Z_z(\mathbf{x}_u) = \frac{1}{2} \int_{z_L}^{z_U} \mathbb{Q} \left\{ \min_{\boldsymbol{\theta}'_u: \mathbf{w}_z^T \boldsymbol{\theta}'_u = z} \sqrt{\sum_{k=1}^{N_A} [f(\mathbf{x}_u, \boldsymbol{\kappa}_k) - f(\mathbf{x}'_u, \boldsymbol{\kappa}'_k)]^2 + \sum_{i=1}^{N_D} [f(\tilde{\mathbf{x}}_i, \boldsymbol{\kappa}_k) - f(\tilde{\mathbf{x}}_i, \boldsymbol{\kappa}'_k)]^2} \right\} |z - z_u| dz \quad (31)$$

The influence of the ambiguity phenomenon intensifies as the SNR diminishes. On another note, the optimization and the integration used in (31) capture the effects of the constraints on  $\mathbf{x}_u^T$  and  $\boldsymbol{\kappa}$ . In extremely low SNR conditions, localization performance is primarily governed by the constraint information. However, in the calculation of CRB, it's challenging to transform a uniform distribution into FIM. For example, as  $\sigma_k$  approaches infinity, the term  $\mathbb{Q}(\cdot)$  in (31) converges to 0.5, leading the ZZB to remain finite, while the CRB tends towards infinity. These factors indicate that, in comparison to the CRB, the ZZB holds the potential for a more accurate depiction of localization performance.

### B. Extrapolated ZZB Based on Q-Function Fitting

Although the ZZB outperforms the CRB in depicting constraint information and nonlinear observation equations, the operation of discarding the integration interval from (68) to (69) results in a ZZB, as shown in (24), that is not sufficiently tight. Considering the case of Gaussian noise, we propose a method that employs the Q-function to approximate the quadrature function outside the well-defined domain, resulting in an EZZB.

*Proposition 5 (EZZB for estimation with Gaussian noise):* Consider an estimation problem for  $\theta \in [\theta_L, \theta_U]$ . The  $i$ -th observation is

$$x_i = f(\theta, \mathbf{t}_i) + \omega_i, \quad (32)$$

where  $\omega_i \sim \mathcal{N}(0, \sigma_i^2)$  is a Gaussian noise. The MSE of any estimator for  $\theta$  satisfies

$$\begin{aligned} \varepsilon(\hat{\theta}) &\geq \frac{1}{2} \int_{\theta_L}^{\theta_U} \mathbb{V}_\theta \left[ \mathbb{Q} \left( \sum_{i=1}^N \frac{|\varphi - \theta|}{2\sigma_i} \right) \right] |\varphi - \theta| d\varphi \\ &\quad + \frac{1}{2} \int_{\theta_U}^{2\theta_U - \theta} \mathbb{Q}[d_U(\varphi + e_U)] |\varphi - \theta| d\varphi \\ &\quad + \frac{1}{2} \int_{2\theta_L - \theta}^{\theta_L} \mathbb{Q}[d_L(\varphi + e_L)] |\varphi - \theta| d\varphi \end{aligned} \quad (33)$$

where  $d_U$  and  $e_U$  are determined by fitting the function to the points  $[\theta_U, \mathbb{Q}(\sum_{i=1}^N \frac{|\theta_U - \theta|}{2\sigma_i})]^T$  and  $[2\theta_U - \theta, \delta]^T$ , and  $d_L$  and  $e_L$  are determined by fitting the function to the points  $[\theta_L, \mathbb{Q}(\sum_{i=1}^N \frac{|\theta_L - \theta|}{2\sigma_i})]^T$  and  $[2\theta_L - \theta, \delta]^T$ .

*Proof:* Please refer to Appendix D.

An example of the quadrature function in the ZZB and its extrapolation in the EZZB, excluding the term  $|\varphi - \theta|$ , is depicted in Fig. 3. Since the entire integration interval is fully considered, the EZZB is tighter than the ZZB. Meanwhile, using a small positive number  $\delta$  in function fitting ensures that the EZZB remains a lower bound. By extending Proposition 5 to the vector cases, we can obtain the EZZB of fingerprint-based localization.

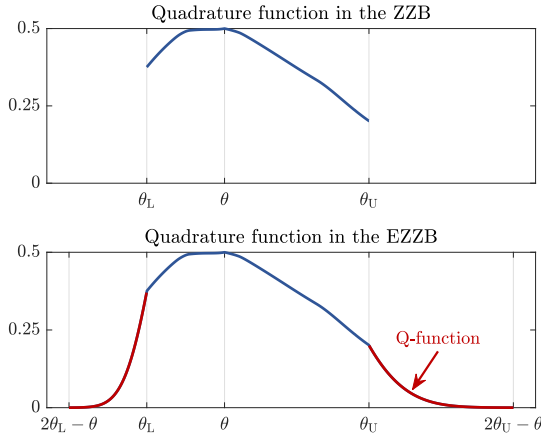


Fig. 3. Quadrature functions in the ZZB and the EZZB, excluding the term  $|\varphi - \theta|$ .

*Proposition 6 (EZZB for fingerprint-based localization):* For the position  $\mathbf{x}_u$ , the MSE of any estimate  $\hat{\mathbf{x}}_u$  satisfies

$$\varepsilon(\hat{\mathbf{x}}_u) \geq Z'_x(\mathbf{x}_u) + Z'_y(\mathbf{x}_u). \quad (34)$$

Using the subscript  $z$  to represent  $x$  or  $y$  uniformly,  $Z_x(\mathbf{x}_u)$  and  $Z_y(\mathbf{x}_u)$  have the following form

$$Z'_z(\mathbf{x}_u) = Z_z(\mathbf{x}_u) + Z_{U,z}(\mathbf{x}_u) + Z_{L,z}(\mathbf{x}_u), \quad (35)$$

where  $Z_z(\mathbf{x}_u)$  is defined as (31). The two adjustment terms are respectively calculated by

$$Z_{U,z}(\mathbf{x}_u) = \frac{1}{2} \int_{z_U}^{2z_U - z} \mathbb{Q}[d_U(z + e_U)] |z - z_u| dz \quad (36)$$

and

$$Z_{L,z}(\mathbf{x}_u) = \frac{1}{2} \int_{2z_L - z}^{z_L} \mathbb{Q}[d_L(z + e_L)] |z - z_u| dz. \quad (37)$$

where  $d_U$ ,  $e_U$ ,  $d_L$  and  $e_L$  are obtained by fitting the Q-function in the same manner as in Proposition 5.

*Proof:* Please refer to Appendices C and D.

## VI. APPROXIMATE MSE OF THE CML ESTIMATOR

To achieve a trade-off between accuracy and complexity in performance analysis, we propose an MSE approximation method based on the suboptimal estimator described in [41]. Considering a position  $\mathbf{x}_u$  in a rectangle  $\mathcal{A}_u$  with dimensions  $[x_L, x_U] \times [y_L, y_U]$ , the possible solutions of (2a) is presented in Fig. 4. The orange dashed curves represent the levels of the objective function (2a). When the unconstrained ML (UML) estimate neglecting the constraints (2b)–(2e) lies outside  $\mathcal{A}_u$ , the optimal CML estimate is a projection of the UML estimate onto the boundaries of  $\mathcal{A}_u$  in a complicated manner [41]. Analyzing the performance of such optimal estimators is generally intractable. An alternative suboptimal estimator

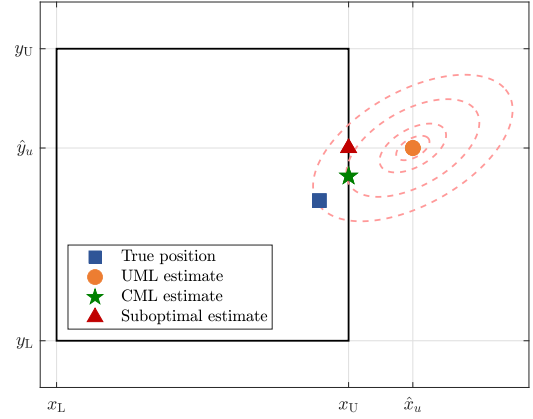


Fig. 4. Some estimates of a position with certain observations.

involves applying the following projection functions to the UML estimate

$$h_x(x) = \begin{cases} x_L, & x < x_L, \\ x, & x_L \leq x \leq x_U, \\ x_U, & x > x_U. \end{cases} \quad h_y(y) = \begin{cases} y_L, & y < y_L, \\ y, & y_L \leq y \leq y_U, \\ y_U, & y > y_U. \end{cases} \quad (38) \quad (39)$$

Subsequently, the MSE of the suboptimal estimator is calculated as

$$\varepsilon(\hat{\mathbf{x}}_u) = \int_{-\infty}^{\infty} \int_{-\infty}^{\infty} \left\{ [h_x(\hat{x}_u) - x_u]^2 + [h_y(\hat{y}_u) - y_u]^2 \right\} \times g(\hat{x}_u, \hat{y}_u) d\hat{x}_u d\hat{y}_u \quad (40)$$

where  $g(\hat{x}_u, \hat{y}_u)$  represents the PDF of the UML estimator. Obtaining the exact expression of  $g(\hat{x}_u, \hat{y}_u)$  is extremely intractable, but fortunately, it is asymptotically equivalent to the PDF of a Gaussian distribution with  $\mathbf{x}_u$  as the mean and  $\mathbf{J}_e^{-1}(\mathbf{x}_u)$  as the variance [25].

By substituting the PDF of the 2-D Gaussian distribution  $\mathcal{N}(\mathbf{x}_u, \mathbf{J}_e^{-1}(\mathbf{x}_u))$  for  $p(\hat{x}_u, \hat{y}_u | \mathbf{x}_u, \boldsymbol{\kappa}, \mathcal{X})$  in (40), we obtain an AMSE of the suboptimal estimator. Since the performance of the suboptimal estimator only slightly degrades compared to the CML solution, (40) can also be regarded as a representative of the AMSE for the CML estimator.

## VII. NUMERICAL RESULTS

We employ numerical simulations to evaluate the proposed bounds for fingerprint-based localization error. In simulations, we construct a 10m  $\times$  10m square room as the area of interest for localization (localization area). The APs are deployed within a 20m  $\times$  20m area centered around the center of the room. The APs within the localization area are considered to have a LoS connection, while those outside are treated as non-LoS (NLoS). The ratio of LoS to NLoS APs is fixed at 1 : 3. The LDPL model parameter  $\alpha$  is set to range between  $-40$  and  $-20$  dBm, while  $\beta$  varies between 1.6 to 2 for LoS and 2 to 44 for NLoS cases. The training data comprises the uniformly sampled RPs on an  $n \times n$  grid, while the RSS readings from

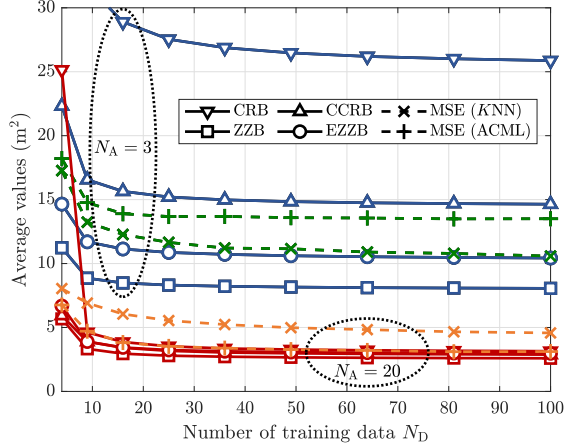


Fig. 5. Evaluation of the proposed bounds versus different  $N_A$  and  $N_D$  with  $\sigma_k = 6$ .

different APs are observed only once at each RP. The test data consists of the points sampled on a  $10 \times 10$  grid. The number of Gauss–Legendre quadrature nodes is set to 100 for the calculation of the ZZB and 200 for the EZZB, respectively, due to their different integration intervals. For the localization algorithms, the Monte Carlo simulations are conducted 1,000 times.

#### A. Tightness of the Proposed Bounds

To verify the tightness of the proposed bounds, we compare them against two localization techniques: the classical KNN algorithm, and an approximate CML (ACML) estimator using the TRR algorithm. In the KNN algorithm, we set  $K = 4$ , a choice that has been demonstrated as optimal in most cases by existing studies. To ensure the identification of the global optimum when solving problem (2) with the TRR algorithm, we use the true values of the unknown parameters as initial values.

While the standard deviation of the observation noise, denoted as  $\sigma_k$ , is set to 6 dBm, we vary the number of APs, denoted by  $N_A$ , and the number of training data, represented as  $N_D$ , in our comparisons. The MSEs of the algorithms and the bounds averaged over 100 instances of test data are illustrated in Fig 5. It is observed that, when both  $N_A$  and  $N_D$  are large, all the proposed lower bounds are able to depict the performance of the ACML estimator. However, when  $N_A$  is small, i.e.  $N_A = 3$ , the CRB and the CCRB significantly overestimate the MSE, and no longer serve as lower bounds. This is attributed to the inadequacy of the Fisher information in capturing constraint knowledge. Nevertheless, with our modifications, the CCRB is more effective than the CRB, especially for cases with a small  $N_D$ , i.e.  $N_D = 4$ . In contrast to the bounds derived from Fisher information, both variants of ZZB consistently serve as lower bound for localization MSE even with small  $N_A$  and  $N_D$ . Meanwhile, the EZZB is tighter than the ZZB.

Keeping  $\sigma_k$  fixed while varying  $N_A$  and  $N_D$  can be regarded as changing the SNR of observation. To more intuitively

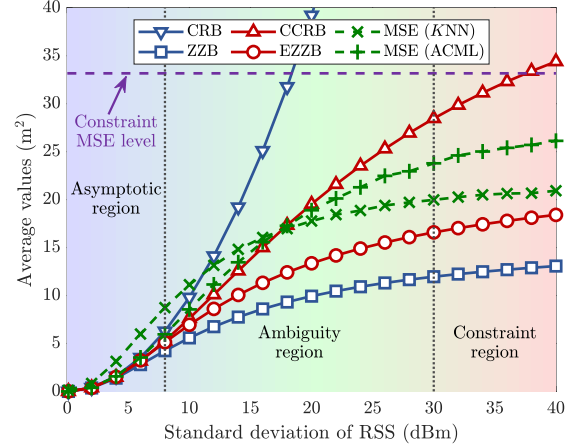


Fig. 6. Evaluation of the proposed bounds versus  $\sigma_k$  within different regions with  $N_A = 20$ ,  $N_D = 25$ .

demonstrate the behavior of the various bounds under different SNRs, we fix  $N_A = 20$  and  $N_D = 25$  and vary the value of  $\sigma_k$ , and present the results in Fig. 6. As the variance of noise increases, we can observe a transition from asymptotic region to ambiguity region, and finally to constraint region (*a priori* region in [36], [37]). The threshold delimiting the constraint region can be defined as the value of  $\sigma_k$  where the EZZB reduces to half of the constraint (*a priori*) performance level [36]. The threshold marking the asymptotic region can be determined by the condition where the EZZB closely matches the CRB [36]. Here, we adopt the value at which the EZZB equals 90% of the CRB. It is noted that the thresholds dividing the three regions are not strict, while the localization error shows a smooth transition within these regions.

As shown in Fig. 6, within the asymptotic region, all the proposed bounds except the CRB are close to the MSE of the ACML estimator, serving as tight lower bounds. The existing literatures suggest the range of  $\sigma_k$  is typically between 3 and 8 [64]. Under these conditions, the estimate operation predominantly lies in the asymptotic region, hence the proposed bounds are almost tight. Within the ambiguity region, we observe that neither the ZZB nor the ACML estimate exhibits the pronounced “peaking” and surpassing of the CRB, in contrast to what is reported in [36]. This suggests that the “localness” of CRB is not the main factor affecting its accuracy in fingerprint-based localization. **Therefore, using constraint knowledge to improve CRB is convincing, which is proved by the values of the CCRB under moderate SNR conditions.** When  $\sigma_k$  is too large, the two bounds based on Fisher information apparently overestimate the localization MSE, even exceeding the constraint MSE level, because they do not capture the constraints on propagation parameters. In contrast, the proposed ZZB and EZZB are effective lower bounds in all three regions.

We can observe from Fig 5 and 6, as a biased estimator, the KNN algorithm could outperform the ACML estimator under poor conditions (characterized by small  $N_A$ , small  $N_D$ , or large  $\sigma_k$ ). It is inspiring that the ZZB and EZZB remain capable of globally characterizing the performance

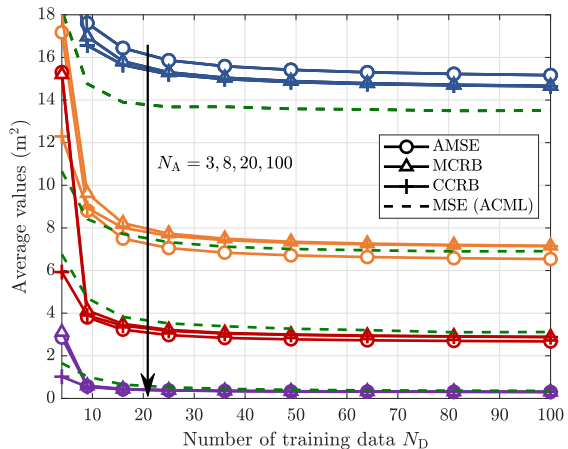


Fig. 7. Evaluation of the proposed AMSE versus different  $N_A$  and  $N_D$  with  $\sigma_k = 6$ .

of this biased estimator. In summary, the proposed EZZB is sufficiently tight in most scenarios, while the other proposed bounds characterize the asymptotic localization performance.

### B. Precision of the Proposed AMSE

To evaluate the accuracy of the proposed AMSE, we compare it with the MSE of the ACML estimator. Considering that the AMSE can only characterize map information, the degenerate version of the CCRB, i.e. the MCRB, is compared. The CCRB is also included in the comparison to illustrate the accuracy loss when only considering map constraints. We present the results under different values of  $N_A$  and  $N_D$ , as shown in Fig. 7. It is observed that when  $N_D = 4$ , only the CCRB that characterizes all the constraints is reliable. As  $N_D$  increases, the MCRB and the CCRB become almost identical, indicating that the map provides the most important constraint information. At lower values of  $N_A$  or  $N_D$ , both the AMSE and the MCRB overestimate the MSE of the ACML estimator. The convergence of the three curves at  $N_A = 100$  indicates that the AMSE is asymptotically precise. Additionally, with smaller  $N_A$  or  $N_D$ , the values of the AMSE tend to be greater than that of the MCRB, and vice versa. This behavior is consistent with the relationship of MSE for estimators with hard-constraints (corresponding to the AMSE) and soft-constraints (corresponding to the MCRB) as reported in [41].

### C. Comparison with Existing Bounds

We compare our work with there existing bounds for fingerprint-based localization error. The first one, referred to as the basic CRB, neglects the impact of training data [26], which essentially represents a bound for RSS range-based localization. The second one, augmenting the basic CRB with the RP position error compensation (RPEC), serves as a modified bound [30]. The third one is tailored for RSS range-based localization with path loss exponent calibration (PLEC) [31], which can also be viewed as a CRB for fingerprint-based localization error.

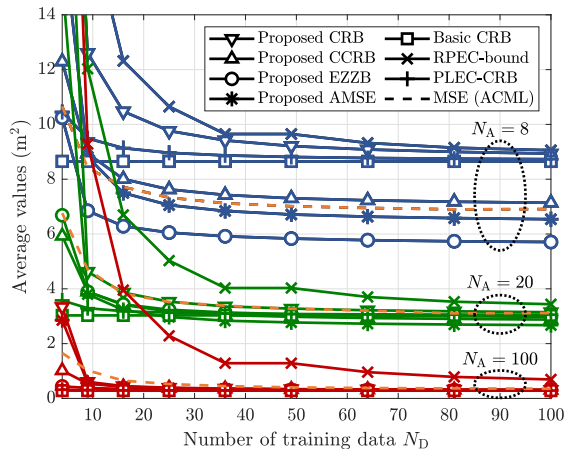


Fig. 8. Comparison of various bounds versus different  $N_A$  and  $N_D$  with  $\sigma_k = 6$ .

As shown in Fig 8, the basic CRB remains constant regardless of changes in the number of training data. Although the RPEC-based bound attempts to depict the relationship between localization performance and the number of RPs, its characterization is notably imprecise. Since the PLEC-based CRB accounts for only one parameter within the signal propagation model, it underestimates the role of training data. The proposed CRB, the RPEC-based bound, and the PLEC-based CRB all converge to the basic CRB as the number of training data approaches infinity. It is observed from the results averaged over the test data, the proposed CCRB and EZZB are the tightest bounds, while the proposed AMSE is almost precise. To better compare the accuracy of the various proposed metrics, we further present them for each set of test data instead of average values in the following subsection.

### D. Numerical Heatmaps

To facilitate a more intuitive and comprehensive comparison, we generate numerical heatmaps for all the bounds, the proposed AMSE, and the MSE of algorithms, as illustrated in Fig 9, where the parameters are set to  $N_A = 8$ ,  $N_D = 16$  and  $\sigma_k = 6$ . Instead of relying on the average results over the test data, the heatmaps yield a detailed visualization of their trends and patterns throughout the room. These heatmaps enable a precise assessment of which metric can serve as the most exact characterization of localization performance.

In comparing the heatmap of the ACML estimator, it is apparent that the proposed CRB, the proposed CCRB, the basic CRB, the RPEC-based bound and the PLEC-based CRB can no longer serve as reliable lower bounds. In these bounds, apart from the RPEC-based bound, the other four exhibit similar patterns because their values are all fundamentally determined by the NRI. Benefiting from the heatmaps, we can observe that although the CCRB and AMSE have similar average values, the AMSE and the MSE of the ACML estimator demonstrate more closely aligned details. This reaffirms that the map is the most crucial constraint, as the AMSE cannot depict other constraints, while the AMSE outperforms the CCRB in portraying

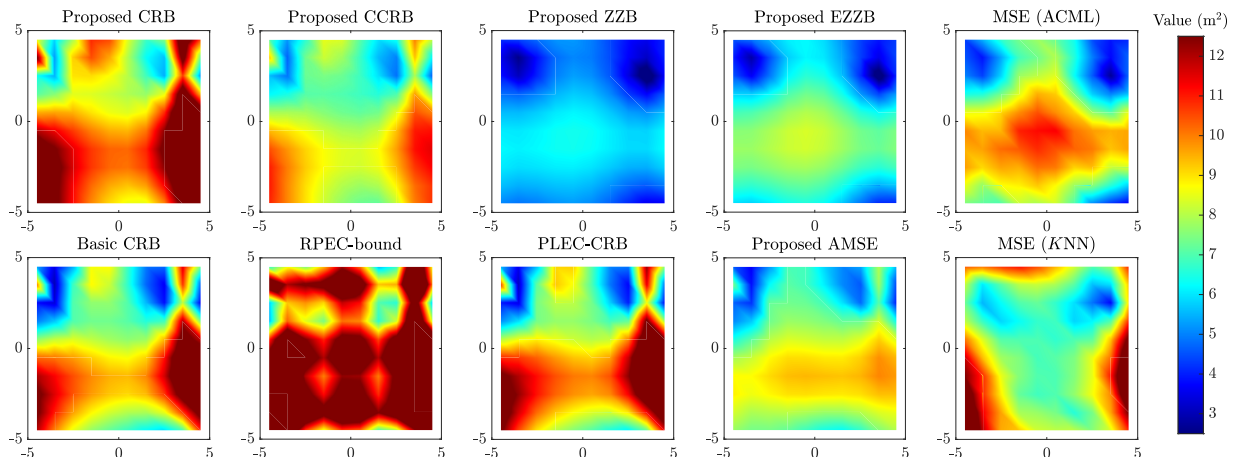


Fig. 9. Heatmaps depicting various metrics and the MSE of algorithms with  $N_A = 8$ ,  $N_D = 16$  and  $\sigma_k = 6$ .

**the map information.** Upon applying the constraint knowledge, the proposed ZZB serves as lower bound, but it lacks the requisite tightness to characterize the localization performance. Both the proposed EZZB and AMSE exhibit details most similar to the MSE of the ACML estimator. Despite a uniform underestimation, the EZZB closely mirrors the MSE in terms of variation patterns. The AMSE shows some inconsistencies with the MSE, which are mainly caused by the nonlinearity of the localization problem. Yet, compared to the EZZB, which requires numerous optimization operations, the AMSE benefits from significantly lower computational complexity, potentially appealing for practical applications. Moreover, although the performance of the biased KNN algorithm is difficult to characterize accurately, the values of the proposed ZZB and EZZB stably maintain lower than the MSEs of the KNN algorithm throughout the localization area.

#### E. Localization Errors with Different $N_A$ and $N_D$

Benefiting from the high accuracy within asymptotic region and the low complexity of the proposed AMSE, we are able to provide some macroscopic numerical results regarding the deployment of localization systems. We conduct 100 Monte Carlo simulations by varying the positions of APs under each fixed set of  $N_A$  and  $N_D$  values with  $\sigma_k = 6$ , and illustrate the contour map of the AMSE as depicted in Fig 10. The contour lines indicate the approximate number of APs and training data required to achieve a certain level of localization accuracy under this noise condition. Since the contour lines merely delineate the lower bound, more APs and training data would actually be needed in practice. The solid red line represents the threshold curve where increasing  $N_D$  beyond a certain  $N_A$  results in less than a 1% decrease in AMSE. The dashed blue line represents the threshold curve where increasing  $N_A$  beyond a certain  $N_D$  yields less than a 1% decrease in AMSE. In this scenario, when  $N_A$  reaches 96 and  $N_D$  reaches 30, further increases in both APs and training data yield marginal gains. This results can be generalized to other scenarios, offering insights into the deployment quantities for APs and training data.

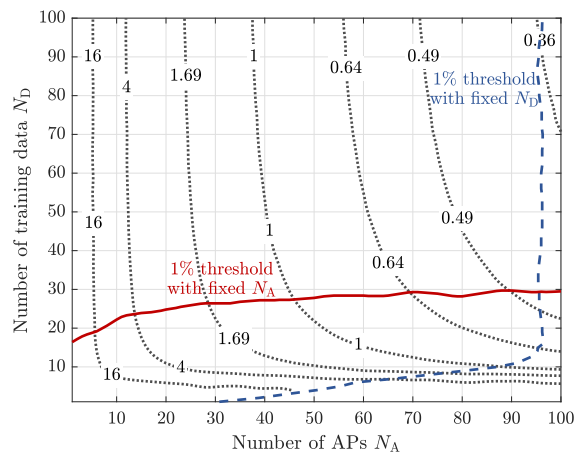


Fig. 10. Contour map of the proposed AMSE by varying  $N_A$  and  $N_D$  with  $\sigma_k = 6$ .

## VIII. EXPERIMENTAL RESULTS

To further verify the proposed performance bounds, we collect Wi-Fi fingerprint data using the Samsung Galaxy S7 smartphones inside a typical office building. To facilitate the collection of fingerprint data, we develop an app for collecting Wi-Fi fingerprints using Android Studio. The scene of data collection and the app are shown in Fig. VIII. Considering the significant differences between LoS and NLoS propagation environments, we select a corridor with a few obstacles where it is easy to determine whether an AP is in LoS as our localization area, having the size of  $32.4 \text{ m} \times 2.8 \text{ m}$ . On a grid with  $0.6 \text{ m}$  intervals, we alternately select 132 RPs and 132 test points, as presented in Fig. 12. At each RP and test point, 40 groups of fingerprint data are collected. To obtain the MSE at the test points, 1000 tests are conducted. In each test, one group is randomly selected from the 40 groups of fingerprint data for each RP and test point.

Among more than 100 APs which can be detected, we select 12 of them and measure their exact positions. Subsequently, we employ all the fingerprint data and the actual position of



Fig. 11. Experimental scene and fingerprint data collection app.

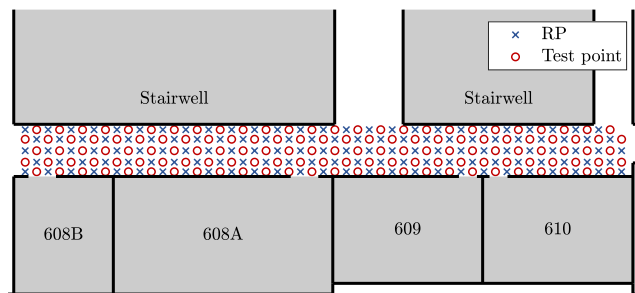


Fig. 12. Localization area, along with the layout of RPs and test points.

an AP to fit the corresponding parameters  $\alpha_k$ ,  $\beta_k$  and  $\sigma_k$  as accurate as possible. For the four LoS APs, the fitted values of  $\alpha_k$ ,  $\beta_k$  and  $\sigma_k$  are in the ranges of  $-49.09 \sim -37.86$ ,  $1.61 \sim 1.88$ , and  $3.78 \sim 6.49$ , respectively. Meanwhile, for the eight NLoS APs, the corresponding value ranges are  $-50.00 \sim -20.00$ ,  $2.23 \sim 5.57$ , and  $4.02 \sim 6.64$ . The lower bounds are calculated by using the precise values of  $a_k$  and  $b_k$ , and the fitted values of  $\alpha_k$ ,  $\beta_k$  and  $\sigma_k$ . The calculated parameter values are consistent with engineering experience [21], [64]. The RSS observations from NLoS APs exhibit greater observation noise compared to those from LoS APs, which aligns with intuitive understanding.

We vary  $N_A$  and  $N_D$  by respectively removing APs and RPs, and present the values averaged over the test data in Fig 13. Since the ACML estimator is sensitive to parameter errors, we only conduct the  $KNN$  algorithm. It is noted that the basic CRB is not affected by variations in training data. As the lower bound for RPEC-based bound, PLEC-based CRB and the proposed CRB, the basic CRB significantly overestimates the MSE, implying that other bounds are even poorer. This is because, in situations with fewer APs, the constraint knowledge is a significant factor affecting the localization performance, and these bounds are unable to depict this information. In contrast, the proposed CCRB, EZZZB and AMSE exhibit values and trends close to the MSE of the  $KNN$  algorithm, effectively characterizing the performance of fingerprint-based localization. Particularly, the EZZZB is tighter than the CCRB under poor conditions. Despite the inaccuracy

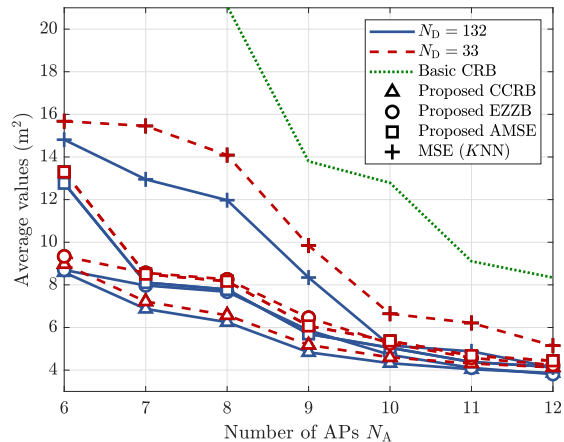


Fig. 13. Evaluation of the proposed metrics versus different  $N_A$  and  $N_D$  based on experimental data.

of model parameters, we can still discern the effectiveness of the proposed metrics in the actual experimental data, which is crucial for data-driven fingerprint-based localization.

## IX. CONCLUSIONS

This paper provides novel metrics for quantitatively analyzing the performance of fingerprint-based indoor localization, including some lower bounds and an approximation of MSE. By deriving the EFIM and its decomposed form based on the LDPL model, we established the CRB. To incorporate constraint knowledge, we developed a CCRB based on an approximation of Fisher information. For better characterization of nonlinear mapping and constraint information, we introduced and refined the ZZB for fingerprint-based localization. The Gauss-Legendre quadrature and the TRR algorithm were used to reduce the computational complexity. By extrapolating the quadrature function beyond its well-defined range through the Q-Function fitting, we developed an EZZZB, which is tighter than the ZZB. For the CML estimator of localization, we proposed an AMSE calculation method based on a suboptimal projection. The simulation and experimental results validated the tightness of the proposed bounds and the precision of the proposed AMSE. This work not only contributes to the theoretical underpinnings of fingerprint-based indoor localization but also paves the way for its practical implementations in the IoT paradigm.

To further advance the research, we identify several pivotal directions for our future work: *Firstly*, we plan to develop new metrics to leverage the information from absent RSS observations by modifying the observation model; *Secondly*, we aim to refine our metrics for multi-room buildings to better depict localization performance through geographic zoning or fingerprint clustering; *Thirdly*, we will explore optimizing localization system deployment using our metrics with convex optimization or heuristic methods; *Fourthly*, we intend to extend the proposed metrics to other problems, establishing a unified theoretical framework for indoor localization.

APPENDIX A  
PROOF OF PROPOSITION 1

The first element of (13) is calculated as

$$\mathbf{J}_{\mathbf{x}_u, \mathbf{x}_u} = \frac{\partial \mathbf{r}_u^T}{\partial \mathbf{x}_u} \mathbf{C}_u^{-1} \frac{\partial \mathbf{r}_u}{\partial \mathbf{x}_u^T}, \quad (41)$$

where the covariance matrix of the RSS observations is

$$\mathbf{C}_u = \text{diag}(\sigma_1^2, \sigma_2^2, \dots, \sigma_{N_A}^2). \quad (42)$$

The Jacobian matrix in (41) can be represented as

$$\frac{\partial \mathbf{r}_u^T}{\partial \mathbf{x}_u} = [\mathbf{u}_{u,1} \quad \mathbf{u}_{u,2} \quad \dots \quad \mathbf{u}_{u,N_A}] \quad (43)$$

According to (1), we have

$$\mathbf{u}_{u,k} = \left[ \frac{10(a_k - x_u)\beta_k}{d_{u,k}^2 \ln 10}, \frac{10(b_k - y_u)\beta_k}{d_{u,k}^2 \ln 10} \right]^T, \quad (44)$$

where  $d_{u,k}^2 = (x_u - a_k)^2 + (y_u - b_k)^2$ . By substituting (42) and (43) into (41), we can obtain

$$\mathbf{J}_{\mathbf{x}_u, \mathbf{x}_u} = \sum_{k=1}^{N_A} \frac{1}{\sigma_k^2} \mathbf{u}_{u,k} \mathbf{u}_{u,k}^T \quad (45)$$

The FIM for  $\boldsymbol{\kappa}_k$  is calculated as

$$\mathbf{J}_{\boldsymbol{\kappa}_k, \boldsymbol{\kappa}_k} = \frac{\partial \mathbf{r}_{:,k}^T}{\partial \boldsymbol{\kappa}_k} (\sigma_k^2 \mathbf{I}_{N_D})^{-1} \frac{\partial \mathbf{r}_{:,k}}{\partial \boldsymbol{\kappa}_k^T}, \quad (46)$$

where  $\mathbf{r}_{:,k}$  is defined by

$$\mathbf{r}_{:,k} = [r_{u,k}, \tilde{r}_{1,k}, \tilde{r}_{2,k}, \dots, \tilde{r}_{N_D,k}]^T. \quad (47)$$

Then, the Jacobian matrix in (46) can be represented as

$$\frac{\partial \tilde{\mathbf{r}}_{:,k}^T}{\partial \boldsymbol{\kappa}_k} = [\mathbf{v}_{u,k} \quad \tilde{\mathbf{v}}_{1,k} \quad \tilde{\mathbf{v}}_{2,k} \quad \dots \quad \tilde{\mathbf{v}}_{N_D,k}] \quad (48)$$

According to (1), we have

$$\mathbf{v}_{u,k} = \left[ 1, -5 \lg d_{u,k}^2, \frac{10(x_u - a_k)\beta_k}{d_{u,k}^2 \ln 10}, \frac{10(y_u - b_k)\beta_k}{d_{u,k}^2 \ln 10} \right]^T, \quad (49)$$

and

$$\tilde{\mathbf{v}}_{i,k} = \left[ 1, -5 \lg \tilde{d}_{i,k}^2, \frac{10(\tilde{x}_i - a_k)\beta_k}{\tilde{d}_{i,k}^2 \ln 10}, \frac{10(\tilde{y}_i - b_k)\beta_k}{\tilde{d}_{i,k}^2 \ln 10} \right]^T. \quad (50)$$

where  $\tilde{d}_{i,k}^2 = (\tilde{x}_i - a_k)^2 + (\tilde{y}_i - b_k)^2$ . By concatenating the column vectors  $\tilde{\mathbf{v}}_{i,k}$  row-wise into a matrix

$$\tilde{\mathbf{V}}_k = [\tilde{\mathbf{v}}_{1,k} \quad \tilde{\mathbf{v}}_{2,k} \quad \dots \quad \tilde{\mathbf{v}}_{N_D,k}], \quad (51)$$

we can transform (46) to

$$\mathbf{J}_{\boldsymbol{\kappa}_k, \boldsymbol{\kappa}_k} = \frac{1}{\sigma_k^2} \left( \mathbf{v}_{u,k} \mathbf{v}_{u,k}^T + \tilde{\mathbf{V}}_k \tilde{\mathbf{V}}_k^T \right). \quad (52)$$

Additionally, we can derive that

$$\mathbf{J}_{\mathbf{x}_u, \boldsymbol{\kappa}_k} = \frac{1}{\sigma_k^2} \mathbf{u}_{u,k} \mathbf{v}_{u,k}^T. \quad (53)$$

Combining (13), (46), (52) and (53), we have

$$\mathbf{J}_e(\mathbf{x}_u) = \sum_{k=1}^{N_A} \frac{\mathbf{u}_{u,k} \mathbf{u}_{u,k}^T}{\sigma_k^2} \left( 1 - \mathbf{v}_{u,k}^T \left( \mathbf{v}_{u,k} \mathbf{v}_{u,k}^T + \tilde{\mathbf{V}}_k \tilde{\mathbf{V}}_k^T \right)^{-1} \mathbf{v}_{u,k} \right). \quad (54)$$

When  $\tilde{\mathbf{V}}_k \tilde{\mathbf{V}}_k^T$  is full rank, according to the Sherman-Morrison formula, (54) can be simplified to

$$\mathbf{J}_e(\mathbf{x}_u) = \sum_{k=1}^{N_A} \frac{\mathbf{u}_{u,k} \mathbf{u}_{u,k}^T}{\sigma_k^2 \left[ 1 + \mathbf{v}_{u,k}^T \left( \tilde{\mathbf{V}}_k \tilde{\mathbf{V}}_k^T \right)^{-1} \mathbf{v}_{u,k} \right]}. \quad (55)$$

The matrix  $\tilde{\mathbf{V}}_k \tilde{\mathbf{V}}_k^T$  being full-rank is equivalent to the matrix  $\tilde{\mathbf{V}}_k$  having a rank of 4. Based on (50), we can ascertain that this requirement is met when *Condition 1* holds.

For the term  $\mathbf{v}_{u,k}^T \left( \tilde{\mathbf{V}}_k \tilde{\mathbf{V}}_k^T \right)^{-1} \mathbf{v}_{u,k}$ , by utilizing block matrix operations, we can further eliminate  $\beta_k$ , resulting in

$$\mathbf{J}_e(\mathbf{x}_u) = \sum_{k=1}^{N_A} \frac{\mathbf{u}_{u,k} \mathbf{u}_{u,k}^T}{\sigma_k^2 \left[ 1 + \mathbf{s}_{u,k}^T \left( \tilde{\mathbf{S}}_k \tilde{\mathbf{S}}_k^T \right)^{-1} \mathbf{s}_{u,k} \right]}, \quad (56)$$

where

$$\mathbf{s}_{u,k} = \left[ 1, -5 \lg d_{u,k}^2, \frac{10(x_u - a_k)}{d_{u,k}^2 \ln 10}, \frac{10(y_u - b_k)}{d_{u,k}^2 \ln 10} \right]^T, \quad (57)$$

$$\tilde{\mathbf{S}}_k = [\tilde{\mathbf{s}}_{1,k} \quad \tilde{\mathbf{s}}_{2,k} \quad \dots \quad \tilde{\mathbf{s}}_{N_D,k}], \quad (58)$$

and

$$\tilde{\mathbf{s}}_{i,k} = \left[ 1, -5 \lg \tilde{d}_{i,k}^2, \frac{10(\tilde{x}_i - a_k)}{\tilde{d}_{i,k}^2 \ln 10}, \frac{10(\tilde{y}_i - b_k)}{\tilde{d}_{i,k}^2 \ln 10} \right]^T. \quad (59)$$

Subsequently, by introducing the definitions of NRI and EoT, we can obtain (14).

APPENDIX B  
PROOF OF PROPOSITION 2

When the observation equation is as shown in (26), the MSE of estimating  $\theta$  can be expressed as

$$\varepsilon(\hat{\theta}) = \int_{\theta_L - \theta}^{\theta_U - \theta} \epsilon^2 p(\epsilon|\theta) d\epsilon, \quad (60)$$

where  $\epsilon = \hat{\theta} - \theta$  denotes the estimation error of the estimator  $\hat{\theta}$ . To obtain a performance bound independent of the specific estimator, we draw upon the analytical insights provided by ZZB.

As for (60), considering the integral part where  $\epsilon > 0$  and using integration by parts, we can obtain

$$\int_0^{\theta_U - \theta} \epsilon^2 p(\epsilon|\theta) d\epsilon \quad (61)$$

$$= \epsilon^2 \Pr(\xi < \epsilon|\theta)|_{\epsilon=0}^{\theta_U - \theta} - 2 \int_0^{\theta_U - \theta} \epsilon \Pr(\xi < \epsilon|\theta) d\epsilon \quad (62)$$

$$= (\theta_U - \theta)^2 \Pr(\xi < \theta_U - \theta|\theta) - (\theta_U - \theta)^2 + 2 \int_0^{\theta_U - \theta} \epsilon \Pr(\xi > \epsilon|\theta) d\epsilon, \quad (63)$$

where  $\xi$  is a random variable representing the estimation error. Since the optimal estimate is definitely less than  $\theta_U$ , it can be considered that the estimation error will not exceed  $\theta_U - \theta$  at most, i.e.,  $\Pr(\xi < \theta_U - \theta) = 1$ . Therefore, we have

$$\int_0^{\theta_U - \theta} \epsilon^2 p(\epsilon|\theta) d\epsilon = 2 \int_0^{\theta_U - \theta} \epsilon \Pr(\xi > \epsilon|\theta) d\epsilon. \quad (64)$$

Subsequently, by using the approximation [36]

$$\Pr(\xi > \epsilon|\theta) \approx \Pr(\xi < -\epsilon|\theta + 2\epsilon), \quad (65)$$

we have

$$\Pr(\xi > \epsilon|\theta) \approx \frac{1}{2} \Pr(\xi > \epsilon|\theta) + \frac{1}{2} \Pr(\xi < -\epsilon|\theta + 2\epsilon). \quad (66)$$

The right side of (66) can be considered as the probability of error for the following binary hypothesis testing problem

$$\begin{aligned} H_0 : x_i &= f(\theta, \mathbf{t}_i) + \omega_i, \quad i = 1, 2, \dots, N \\ H_1 : x_i &= f(\theta + 2\epsilon, \mathbf{t}_i) + \omega_i, \quad i = 1, 2, \dots, N \end{aligned} \quad (67)$$

with  $\Pr(H_0) = \Pr(H_1) = 0.5$ . Consequently, we can obtain the following inequality

$$\int_0^{\theta_U - \theta} \epsilon^2 p(\epsilon|\theta) d\epsilon \geq 2 \int_0^{\theta_U - \theta} \epsilon P_{\min}(\theta, \theta + 2\epsilon) d\epsilon, \quad (68)$$

where  $P_{\min}(\theta, \theta + 2\epsilon)$  denotes the minimum probability of error for the problem (67) based on the optimal detection criterion. It should be noted that the hypothesis  $H_1$  in (67) is related to  $f(\theta + 2\epsilon, \mathbf{t}_i)$ , and the function  $f(\theta + 2\epsilon, \mathbf{t}_i)$  is well-defined only when  $\theta + 2\epsilon \leq \theta_U$ , i.e.,  $\epsilon \leq (\theta_U - \theta)/2$ . Consequently, the integration interval in (68) is halved, resulting in the following inequality

$$\int_0^{\theta_U - \theta} \epsilon^2 p(\epsilon|\theta) d\epsilon \geq 2 \int_0^{\frac{\theta_U - \theta}{2}} \epsilon P_{\min}(\theta, \theta + 2\epsilon) d\epsilon. \quad (69)$$

Similarly, the integral part for  $\epsilon < 0$  in (60) can be written as

$$\int_{\theta_L - \theta}^0 \epsilon^2 p(\epsilon|\theta) d\epsilon = 2 \int_{\theta_L - \theta}^0 |\epsilon| \Pr(\xi < \epsilon|\theta) d\epsilon. \quad (70)$$

Utilizing the approximation

$$\Pr(\xi < \epsilon|\theta) \approx \Pr(\xi > -\epsilon|\theta + 2\epsilon), \quad (71)$$

we have

$$\int_{\theta_L - \theta}^0 \epsilon^2 p(\epsilon|\theta) d\epsilon \geq 2 \int_{\frac{\theta_L - \theta}{2}}^0 |\epsilon| P_{\min}(\theta, \theta + 2\epsilon) d\epsilon. \quad (72)$$

By combining (69) and (72), and introducing the substitution  $\varphi = \theta + 2\epsilon$ , we can obtain the following inequality

$$\varepsilon(\hat{\theta}) \geq \frac{1}{2} \int_{\theta_L}^{\theta_U} P_{\min}(\theta, \varphi) |\varphi - \theta| d\varphi. \quad (73)$$

Revisiting (64) and (70), we note that for both  $\Pr(\xi > \epsilon|\theta)$  and  $\Pr(\xi < \epsilon|\theta)$ , the closer  $\epsilon$  approaches zero, the greater they become. Consequently, the corresponding minimum probability,  $P_{\min}(\theta, \theta + 2\epsilon)$ , should also increase as  $\epsilon$  approaches zero. This suggests that the function of  $\varphi$ , expressed in the form of  $P_{\min}(\theta, \varphi)$ , is non-increasing on both sides of  $\theta$ . Hence,

we introduce a ‘‘valley-filling’’ function to further improve the inequality. Diverging from the classical definition, our valley-filling function is a symmetric operator with respect to  $\theta$ , defined as

$$\mathbb{V}_\theta[f(x)] = \begin{cases} \max_{\xi: \xi \geq 0} f(x + \xi), & x \geq \theta, \\ \max_{\xi: \xi \geq 0} f(x - \xi), & x < \theta. \end{cases} \quad (74)$$

Applying the modified valley-filling function to (73), we are able to obtain the expression of ZZB as shown in (24).

#### APPENDIX C PROOF OF PROPOSITION 4

To apply Proposition 3 to derive the ZZB of fingerprint-based localization, we first define the function

$$f(\mathbf{x}_i, \boldsymbol{\kappa}_k) = \alpha_k - 5\beta_k \lg \left[ (x_i - a_k)^2 + (y_i - b_k)^2 \right]. \quad (75)$$

According to (1), we can construct the following binary hypothesis testing problem

$$\begin{aligned} H_0 : \tilde{r}_{i,k} &= f(\tilde{\mathbf{x}}_i, \boldsymbol{\kappa}_k) + \omega_k \quad (i = 1, 2, \dots, N_D), \\ r_{u,k} &= f(\mathbf{x}_u, \boldsymbol{\kappa}_k) + \omega_k, \quad k = 1, 2, \dots, N_A \\ H_1 : \tilde{r}_{i,k} &= f(\tilde{\mathbf{x}}_i, \boldsymbol{\kappa}'_k) + \omega_k \quad (i = 1, 2, \dots, N_D), \\ r_{u,k} &= f(\mathbf{x}'_u, \boldsymbol{\kappa}'_k) + \omega_k, \quad k = 1, 2, \dots, N_A \end{aligned} \quad (76)$$

where  $\mathbf{x}'_u = [x'_u, y'_u]^T$  and  $\boldsymbol{\kappa}'_k = [\alpha'_k, \beta'_k, a'_k, b'_k]^T$ . Since  $\omega_k$  is assumed to be Gaussian white noise, we can present the minimum probability of error for this testing problem as (77). In (77),  $\mathbb{Q}(\cdot)$  denotes the Q-function, and the column vector  $\boldsymbol{\theta}'_u$  is formed by concatenating  $\mathbf{x}'_u$  and  $\boldsymbol{\kappa}'_k$ . Since the Q-function is a monotonically decreasing function, the maximization operation in (27) can be transformed into a minimization operation within the Q-function, to reduce the computational complexity. Therefore, we can obtain the expression (31).

#### APPENDIX D PROOF OF PROPOSITION 5

Considering the case of  $\epsilon > 0$ , to address the issue that  $P_{\min}(\theta, \theta + 2\epsilon)$  is not well-defined for  $\epsilon > \frac{\theta_U - \theta}{2}$ , we return to the MSE expression represented by (64). When the noise follows a Gaussian distribution and the observation equation is linear, the probability  $\Pr(\xi > \epsilon|\theta)$  takes the form of the Q-function. Meanwhile, when the observation equation is nonlinear, approximating  $\Pr(\xi > \epsilon|\theta)$  with the Q-function becomes a reluctant but sub-optimal choice. Therefore, we assume the probability has the following form

$$\Pr(\xi > \epsilon|\theta) \approx \mathbb{Q}[d_U(\theta + 2\epsilon + e_U)]. \quad (78)$$

To determine the values of  $d_U$  and  $e_U$ , we need to fit this function to two sets of data. Considering the continuity of the quadrature function, using  $\epsilon = (\theta_U - \theta)/2$  and the corresponding well-defined  $P_{\min}(\theta, \theta_U)$  as one set is a natural choice. The second set comes from an assumption that at the boundary, specifically at  $\epsilon = \theta_U - \theta$ , the probability  $\Pr(\xi > \epsilon|\theta)$  approaches zero. To ensure that the fitting is feasible, we choose a small positive number  $\delta$  close to zero for  $\Pr(\xi > \epsilon|\theta)$  at the boundary, such as  $10^{-4}$ .

$$P_{\min}(\theta_u, \theta'_u) = \mathbb{Q} \left\{ \sqrt{\frac{\sum_{k=1}^{N_A} [f(\mathbf{x}_u, \boldsymbol{\kappa}_k) - f(\mathbf{x}'_u, \boldsymbol{\kappa}'_k)]^2 + \sum_{i=1}^{N_D} [f(\tilde{\mathbf{x}}_i, \boldsymbol{\kappa}_k) - f(\tilde{\mathbf{x}}_i, \boldsymbol{\kappa}'_k)]^2}{4\sigma_k^2}} \right\}. \quad (77)$$

The same procedure is applied for the case of  $\epsilon < \frac{\theta_L - \theta}{2}$  to obtain

$$\begin{aligned} \Pr(\xi < \epsilon|\theta) &\approx 1 - \mathbb{Q}[-d_L(\theta + 2\epsilon + e_L)] \\ &= \mathbb{Q}[d_L(\theta + 2\epsilon + e_L)] \end{aligned} \quad (79)$$

Applying the substitution  $\varphi = \theta + 2\epsilon$  to (78) and (79), and combining them with (24), we can obtain the expression of EZZB as presented in (33).

## REFERENCES

- [1] P. S. Farahsari, A. Farahzadi, J. Rezaezadeh, and A. Bagheri, "A survey on indoor positioning systems for IoT-based applications," *IEEE Internet Things J.*, pp. 1–1, 2022.
- [2] R. S. Shit, S. Sharma, D. Puthal, and A. Y. Zomaya, "Location of things (LoT): A review and taxonomy of sensors localization in IoT infrastructure," *IEEE Commun. Surveys Tuts.*, vol. 20, no. 3, pp. 2028–2061, 3rd Quart. 2018.
- [3] S. He, S.-H. G. Chan, L. Yu, and N. Liu, "Maxlifd: Joint maximum likelihood localization fusing fingerprints and mutual distances," *IEEE Trans. Mobile Comput.*, vol. 18, no. 3, pp. 602–617, Mar. 2019.
- [4] J. Choi, G. Lee, S. Choi, and S. Bahk, "Smartphone based indoor path estimation and localization without human intervention," *IEEE Trans. Mobile Comput.*, vol. 21, no. 2, pp. 681–695, Feb. 2022.
- [5] Y. Xiong, F. Liu, Y. Cui, W. Yuan, T. X. Han, and G. Caire, "On the fundamental tradeoff of integrated sensing and communications under Gaussian channels," *IEEE Trans. Inf. Theory*, vol. 69, no. 9, pp. 5723–5751, Sep. 2023.
- [6] S. He and S.-H. G. Chan, "Wi-Fi fingerprint-based indoor positioning: Recent advances and comparisons," *IEEE Commun. Surveys Tuts.*, vol. 18, no. 1, pp. 466–490, 1st Quart. 2016.
- [7] X. Zhu, W. Qu, T. Qiu, L. Zhao, M. Atiquzzaman, and D. O. Wu, "Indoor intelligent fingerprint-based localization: Principles, approaches and challenges," *IEEE Commun. Surveys Tuts.*, vol. 22, no. 4, pp. 2634–2657, 4th Quart. 2020.
- [8] A. Yassin, Y. Nasser, M. Awad, A. Al-Dubai, R. Liu, C. Yuen, R. Raulefs, and E. Aboutanios, "Recent advances in indoor localization: A survey on theoretical approaches and applications," *IEEE Commun. Surveys Tuts.*, vol. 19, no. 2, pp. 1327–1346, 2nd Quart. 2017.
- [9] Y. Xu, Y. S. Shmaliy, Y. Li, X. Chen, and H. Guo, "Indoor INS/LiDAR-based robot localization with improved robustness using cascaded FIR filter," *IEEE Access*, vol. 7, pp. 34 189–34 197, 2019.
- [10] Y. Xu, Y. S. Shmaliy, Y. Li, and X. Chen, "UWB-based indoor human localization with time-delayed data using EFIR filtering," *IEEE Access*, vol. 5, pp. 16 676–16 683, 2017.
- [11] Y. Yu, R. Chen, L. Chen, X. Zheng, D. Wu, W. Li, and Y. Wu, "A novel 3-D indoor localization algorithm based on BLE and multiple sensors," *IEEE Internet Things J.*, vol. 8, no. 11, pp. 9359–9372, Jun. 2021.
- [12] J. Niu, B. Wang, L. Shu, T. Q. Duong, and Y. Chen, "ZIL: An energy-efficient indoor localization system using ZigBee radio to detect WiFi fingerprints," *IEEE J. Sel. Areas Commun.*, vol. 33, no. 7, pp. 1431–1442, Jul. 2015.
- [13] P. Bahl and V. N. Padmanabhan, "RADAR: An in-building RF-based user location and tracking system," in *Proc. IEEE INFOCOM*, vol. 2, Tel Aviv, Israel, Mar. 2000, pp. 775–784.
- [14] G. Huang, Z. Hu, J. Wu, H. Xiao, and F. Zhang, "WiFi and vision-integrated fingerprint for smartphone-based self-localization in public indoor scenes," *IEEE Internet Things J.*, vol. 7, no. 8, pp. 6748–6761, Aug. 2020.
- [15] L. Yang, N. Wu, B. Li, W. Yuan, and L. Hanzo, "Indoor localization based on factor graphs: A unified framework," *IEEE Internet Things J.*, vol. 10, no. 5, pp. 4353–4366, Mar. 2023.
- [16] B. Ferris, D. Fox, and N. D. Lawrence, "WiFi-SLAM using Gaussian process latent variable models," in *Proc. IJCAI*, Hyderabad, India, Jan. 2007, pp. 2480–2485.
- [17] X. Wang, X. Wang, S. Mao, J. Zhang, S. C. G. Periaswamy, and J. Patton, "Indoor radio map construction and localization with deep Gaussian processes," *IEEE Internet Things J.*, vol. 7, no. 11, pp. 11 238–11 249, Nov. 2020.
- [18] C. Wu, Z. Yang, and Y. Liu, "Smartphones based crowdsourcing for indoor localization," *IEEE Trans. Mobile Comput.*, vol. 14, no. 2, pp. 444–457, Feb. 2015.
- [19] S. Jung, B. Moon, and D. Han, "Unsupervised learning for crowdsourced indoor localization in wireless networks," *IEEE Trans. Mobile Comput.*, vol. 15, no. 11, pp. 2892–2906, Nov. 2016.
- [20] J. Zou, X. Guo, L. Li, S. Zhu, and X. Feng, "Deep regression model for received signal strength based WiFi localization," in *Proc. IEEE DSP*, Shanghai, China, 2018, pp. 1–4.
- [21] A. Goldsmith, *Wireless Communications*. Cambridge Univ. Press, 2005.
- [22] K. Chintalapudi, A. P. Iyer, and V. N. Padmanabhan, "Indoor localization without the pain," in *Proc. ACM MobiCom*, Chicago, IL, USA, Sep. 2010, pp. 173–184.
- [23] Y. Shen and M. Z. Win, "Fundamental limits of wideband localization—part I: A general framework," *IEEE Trans. Inf. Theory*, vol. 56, no. 10, pp. 4956–4980, Oct. 2010.
- [24] Y. Xiong, N. Wu, Y. Shen, and M. Z. Win, "Cooperative localization in massive networks," *IEEE Trans. Inf. Theory*, vol. 68, no. 2, pp. 1237–1258, Feb. 2022.
- [25] S. M. Kay, *Fundamentals of Statistical Signal Processing: Estimation Theory*. Prentice-Hall, 1993.
- [26] B. Huang, M. Liu, Z. Xu, and B. Jia, "On the performance analysis of WiFi based localization," in *Proc. IEEE ICASSP*, Calgary, AB, Canada, 2018, pp. 4369–4373.
- [27] Q. Li, W. Li, W. Sun, J. Li, and Z. Liu, "Cramér-Rao bound analysis of Wi-Fi indoor localization using fingerprint and assistant nodes," in *Proc. IEEE VTC-Fall*, Toronto, ON, Canada, Sep. 2017, pp. 1–5.
- [28] X. Li and B. Huang, "A theoretical analysis on site survey in WiFi fingerprint-based localization," in *Proc. CCDC*, Kunming, China, 2021, pp. 5608–5613.
- [29] B. Huang, R. Yang, B. Jia, W. Li, and G. Mao, "A theoretical analysis on sampling size in wifi fingerprint-based localization," *IEEE Trans. Veh. Technol.*, vol. 70, no. 4, pp. 3599–3608, Apr. 2021.
- [30] Q. Pu, J. K.-Y. Ng, and M. Zhou, "Fingerprint-based localization performance analysis: From the perspectives of signal measurement and positioning algorithm," *IEEE Trans. Instrum. Meas.*, vol. 70, pp. 1–15, 2021.
- [31] B. Zhou, H. C. So, and S. Mumtaz, "Effect of signal propagation model calibration on localization performance limits for wireless sensor networks," *IEEE Trans. Wireless Commun.*, vol. 20, no. 5, pp. 3254–3268, May 2021.
- [32] F. Montorsi, S. Mazuelas, G. M. Vitetta, and M. Z. Win, "On the performance limits of map-aware localization," *IEEE Trans. Inf. Theory*, vol. 59, no. 8, pp. 5023–5038, Aug. 2013.
- [33] R. Sari and H. Zayyani, "RSS localization using unknown statistical path loss exponent model," *IEEE Commun. Lett.*, vol. 22, no. 9, pp. 1830–1833, Sep. 2018.
- [34] J. D. Gorman and A. O. Hero, "Lower bounds for parametric estimation with constraints," *IEEE Trans. Inf. Theory*, vol. 36, no. 6, pp. 1285–1301, Nov. 1990.
- [35] P. Stoica and B. C. Ng, "On the Cramer-Rao bound under parametric constraints," *IEEE Signal Process. Lett.*, vol. 5, no. 7, pp. 177–179, Jul. 1998.
- [36] A. Mallat, S. Gezici, D. Dardari, C. Craeye, and L. Vandendorpe, "Statistics of the MLE and approximate upper and lower bounds—part I: Application to TOA estimation," *IEEE Trans. Signal Process.*, vol. 62, no. 21, pp. 5663–5676, Nov. 2014.
- [37] K. Bell, Y. Steinberg, Y. Ephraim, and H. Van Trees, "Extended Ziv-Zakai lower bound for vector parameter estimation," *IEEE Trans. Inf. Theory*, vol. 43, no. 2, pp. 624–637, Mar. 1997.
- [38] X. Tian, R. Shen, D. Liu, Y. Wen, and X. Wang, "Performance analysis of RSS fingerprinting based indoor localization," *IEEE Trans. Mobile Comput.*, vol. 16, no. 10, pp. 2847–2861, Oct. 2017.

- [39] M. Crowder, "On constrained maximum likelihood estimation with non-i.i.d. observations," *Ann. Inst. Statistical Math.*, vol. 36, no. 1, pp. 239–249, Jul. 1984.
- [40] T. J. Moore, B. M. Sadler, and R. J. Kozick, "Maximum-likelihood estimation, the Cramér–Rao bound, and the method of scoring with parameter constraints," *IEEE Trans. Signal Process.*, vol. 56, no. 3, pp. 895–908, Mar. 2008.
- [41] A. Benavoli, L. Chisci, A. Farina, L. Ortenzi, and G. Zappa, "Hard-constrained versus soft-constrained parameter estimation," *IEEE Trans. Aerosp. Electron. Syst.*, vol. 42, no. 4, pp. 1224–1239, Oct. 2006.
- [42] G. H. Golub and J. H. Welsch, "Calculation of Gauss quadrature rules," *Math. Computation*, vol. 23, no. 106, pp. 221–230, 1969.
- [43] T. F. Coleman and Y. Li, "An interior trust region approach for nonlinear minimization subject to bounds," *SIAM J. Optim.*, vol. 6, no. 2, pp. 418–445, 1996.
- [44] S. He and S.-H. G. Chan, "Sectjunction: Wi-Fi indoor localization based on junction of signal sectors," in *Proc. IEEE ICC*, Sydney, NSW, Australia, 2014, pp. 2605–2610.
- [45] Y. Wei, S.-H. Hwang, and S.-M. Lee, "IoT-aided fingerprint indoor positioning using support vector classification," in *Proc. ICTC*, Jeju, Korea (South), 2018, pp. 973–975.
- [46] O. Altay and M. Ulas, "Location determination by processing signal strength of wi-fi routers in the indoor environment with linear discriminant classifier," in *Proc. ISDFS*, Antalya, Turkey, 2018, pp. 1–4.
- [47] M. Youssef and A. K. Agrawala, "The Horus WLAN location determination system," in *Proc. ACM MobiSys*, Seattle, WA, USA, Jun. 2005, pp. 205–218.
- [48] A. Alhammedi, S. Alraih, F. Hashim, and M. F. A. Rasid, "Robust 3D indoor positioning system based on radio map using Bayesian network," in *Proc. IEEE WF-IoT*, Limerick, Ireland, 2019, pp. 107–110.
- [49] W.-Y. Lin, C.-C. Huang, N.-T. Duc, and H.-N. Manh, "Wi-Fi indoor localization based on multi-task deep learning," in *Proc. IEEE DSP*, Shanghai, China, 2018, pp. 1–5.
- [50] B. Jang and H. Kim, "Indoor positioning technologies without offline fingerprinting map: A survey," *IEEE Commun. Surveys Tuts.*, vol. 21, no. 1, pp. 508–525, 1st Quart. 2019.
- [51] Y. Zhao, Z. Zhang, T. Feng, W. C. Wong, and H. K. Garg, "GraphIPS: Calibration-free and map-free indoor positioning using smartphone crowdsourced data," *IEEE Internet Things J.*, vol. 8, no. 1, pp. 393–406, Jan. 2021.
- [52] A. Rai, K. K. Chintalapudi, V. N. Padmanabhan, and R. Sen, "Zee: Zero-effort crowdsourcing for indoor localization," in *Proc. ACM MobiCom*, Istanbul, Turkey, Aug. 2012, pp. 293–304.
- [53] Y. Han, Y. Shen, X.-P. Zhang, M. Z. Win, and H. Meng, "Performance limits and geometric properties of array localization," *IEEE Trans. Inf. Theory*, vol. 62, no. 2, pp. 1054–1075, Feb. 2016.
- [54] Y. Shen, H. Wymeersch, and M. Z. Win, "Fundamental limits of wideband localization—part II: Cooperative networks," *IEEE Trans. Inf. Theory*, vol. 56, no. 10, pp. 4981–5000, Oct. 2010.
- [55] N. Patwari and A. O. Hero III, "Using proximity and quantized RSS for sensor localization in wireless networks," in *Proc. ACM WSNA*, New York, NY, USA, 2003, pp. 20–29.
- [56] M. Angjelichinoski, D. Denkovski, V. Atanasovski, and L. Gavrilovska, "Cramér–Rao lower bounds of RSS-based localization with anchor position uncertainty," *IEEE Trans. Inf. Theory*, vol. 61, no. 5, pp. 2807–2834, May 2015.
- [57] F. Zhou, L. Fan, J. Tang, and W. Chen, "Placement and concise MSE lower-bound for UAV-enabled localization via RSS," *IEEE Trans. Veh. Technol.*, vol. 71, no. 2, pp. 2209–2213, Feb. 2022.
- [58] K. Kaemarungsi and P. Krishnamurthy, "Modeling of indoor positioning systems based on location fingerprinting," in *Proc. IEEE INFOCOM*, vol. 2, Hong Kong, China, 2004, pp. 1012–1022.
- [59] N. Swangmuang and P. Krishnamurthy, "Location fingerprint analyses toward efficient indoor positioning," in *Proc. IEEE PerCom*, Hong Kong, China, 2008, pp. 100–109.
- [60] C. Zhou, J. Liu, M. Sheng, Y. Zheng, and J. Li, "Exploiting fingerprint correlation for fingerprint-based indoor localization: A deep learning based approach," *IEEE Trans. Veh. Technol.*, vol. 70, no. 6, pp. 5762–5774, Jun. 2021.
- [61] Z. Zhang, Z. Shi, C. Zhou, C. Yan, and Y. Gu, "Ziv-zakai bound for compressive time delay estimation," *IEEE Trans. Signal Process.*, vol. 70, pp. 4006–4019, 2022.
- [62] Z. Yang and Y. Liu, "Understanding node localizability of wireless ad hoc and sensor networks," *IEEE Trans. Mobile Comput.*, vol. 11, no. 8, pp. 1249–1260, Aug. 2012.
- [63] A. Gusi-Amigó, P. Closas, A. Mallat, and L. Vandendorpe, "Ziv-Zakai bound for direct position estimation," *Navig.*, vol. 65, no. 3, pp. 463–475, Oct. 2018.
- [64] "Guidelines for evaluation of radio interface technologies for IMT-advanced," International Telecommunication Union (ITU), Tech. Rep. ITU-R M.2135-1, Dec. 2009. [Online]. Available: [https://www.itu.int/dms\\_pub/itu-r/otp/rep/R-REP-M.2135-1-2009-PDF-E.pdf](https://www.itu.int/dms_pub/itu-r/otp/rep/R-REP-M.2135-1-2009-PDF-E.pdf)